

2

NAVAL POSTGRADUATE SCHOOL

Monterey, California

AD-A203 953



THESIS

DTIC
ELECTE
4 FEB 1989
S D
E

DESIGN OF A THREE-AXIS STABILIZED ORION
SATELLITE USING AN ALL-THRUSTER
CONTROL SYSTEM

by

Suzanne M. Dee

December 1988

Thesis Advisor:

H. A. Titus

Approved for public release; distribution is unlimited.

89 2 13 220

REPORT DOCUMENTATION PAGE

1a. REPORT SECURITY CLASSIFICATION UNCLASSIFIED		1b. RESTRICTIVE MARKINGS	
2a. SECURITY CLASSIFICATION AUTHORITY		3. DISTRIBUTION/AVAILABILITY OF REPORT Approved for public release; distribution is unlimited.	
2b. DECLASSIFICATION/DOWNGRADING SCHEDULE		5. MONITORING ORGANIZATION REPORT NUMBER(S)	
4. PERFORMING ORGANIZATION REPORT NUMBER(S)		7a. NAME OF MONITORING ORGANIZATION Naval Postgraduate School	
6a. NAME OF PERFORMING ORGANIZATION Naval Postgraduate School	6b. OFFICE SYMBOL (If applicable) Code 39	7b. ADDRESS (City, State, and ZIP Code) Monterey, CA 93943-5000	
6c. ADDRESS (City, State, and ZIP Code) Monterey, CA 93943-5000		9. PROCUREMENT INSTRUMENT IDENTIFICATION NUMBER	
8a. NAME OF FUNDING/SPONSORING ORGANIZATION	8b. OFFICE SYMBOL (If applicable)	10. SOURCE OF FUNDING NUMBERS	
8c. ADDRESS (City, State, and ZIP Code)		PROGRAM ELEMENT NO.	PROJECT NO.
		TASK NO.	WORK UNIT ACCESSION NO.
11. TITLE (Include Security Classification) DESIGN OF A THREE-AXIS STABILIZED ORION SATELLITE USING AN ALL-THRUSTER ATTITUDE CONTROL SYSTEM			
12. PERSONAL AUTHOR(S) Suzanne M. Dee			
13a. TYPE OF REPORT Master's Thesis	13b. TIME COVERED FROM TO	14. DATE OF REPORT (Year, Month, Day) December 1988	15. PAGE COUNT 116
16. SUPPLEMENTARY NOTATION The view expressed in this thesis are those of the author and do not reflect the official policy or position of the Department of Defense or the U.S. Government			
17. COSATI CODES		18. SUBJECT TERMS (Continue on reverse if necessary and identify by block number)	
FIELD	GROUP	SUB-GROUP	
		Satellite, Lightsat, Orion, Naval Postgraduate School, Three-Axis Stabilization, All-Thruster Attitude Control, Get-Away Special <i>Thesis. (M)M</i>	
19. ABSTRACT (Continue on reverse if necessary and identify by block number) An all-thruster three-axis stabilized attitude control system has been designed for the Naval Postgraduate School (NPS) satellite bus, ORION. The satellite is a cylinder, 19 inches in diameter, 35 inches in length, 250 pounds maximum mass with 32 pounds for payloads. ORION will be ejected from an extended Get-Away-Special (GAS) canister. Launch from any GAS can configured expendable booster or the space shuttle is assumed. The minimization techniques of Pontryagin have been used to derive control laws that support fuel efficient operation. A minimum time cost function is applied in the acquisition phase to reduce rates to acceptable levels. A weighted minimum fuel-time cost function is used during the on-station phase. Bang-Off-Bang control with two switching curves is employed outside of a boundary region. Inside the boundary region, four pulse limit cycle control with time constants on the order of 100 seconds is applied. Lifetimes in the			
20. DISTRIBUTION/AVAILABILITY OF ABSTRACT <input checked="" type="checkbox"/> UNCLASSIFIED/UNLIMITED <input type="checkbox"/> SAME AS RPT. <input type="checkbox"/> DTIC USERS		21. ABSTRACT SECURITY CLASSIFICATION Unclassified	
22a. NAME OF RESPONSIBLE INDIVIDUAL Prof. Hal A. Titus		22b. TELEPHONE (Include Area Code) (408) 646-2560	22c. OFFICE SYMBOL Code 62Ts

Item 19 Continued:

range of 4 to 28 months are obtained utilizing these techniques.

Approved for public release; distribution unlimited

Design of a Three-Axis Stabilized ORION Satellite
Using an All-Thruster
Attitude Control System

by

Suzanne M. Dee
Lieutenant, United States Navy
B.S., United States Naval Academy, 1981

Submitted in partial fulfillment of the
requirements for the degree of

MASTER OF SCIENCE IN ELECTRICAL ENGINEERING

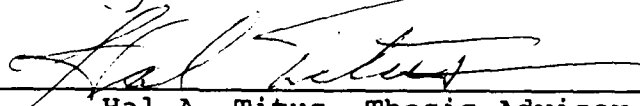
from the


NAVAL POSTGRADUATE SCHOOL
December 1988


Author:



Suzanne M. Dee

Approved by:


Hal A. Titus, Thesis Advisor


Jeffrey Burl, Second Reader


John P. Powers, Chairman
Department of Electrical and Computer Engineering


Gordon E. Schacher,
Dean of Science and Engineering

ABSTRACT

An all-thruster three-axis stabilized attitude control system has been designed for the Naval Postgraduate School (NPS) satellite bus, ORION. The satellite is a cylinder, 19 inches in diameter, 35 inches in length, 250 pounds maximum mass with 32 pounds for payloads. ORION will be ejected from an extended Get-Away-Special (GAS) canister. Launch from any GAS can configured expendable booster or the space shuttle is assumed. The minimization techniques of Pontryagin have been used to derive control laws that support fuel efficient operation. A minimum time cost function is applied in the acquisition phase to reduce rates to acceptable levels. A weighted minimum fuel-time cost function is used during the on-station phase. Bang-Off-Bang control with two switching curves is employed outside of a boundary region. Inside the boundary region, four-pulse limit cycle control with time constants on the order of 100 seconds is applied. Lifetimes in the range of 4 to 28 months are obtained utilizing these techniques.

THESIS DISCLAIMER

The reader is cautioned that computer programs developed in this research may not have been exercised for all cases of interest. While every effort has been made, within the time available, to ensure that the programs are free of computational and logic errors, they cannot be considered validated. Any application of these programs without additional verification is at the risk of the user.

Accession For	
NTIS GRA&I	<input checked="" type="checkbox"/>
DTIC TAB	<input type="checkbox"/>
Unannounced	<input type="checkbox"/>
Justification	
By _____	
Distribution/	
Availability Codes	
Dist	Avail and/or Special
A-1	



TABLE OF CONTENTS

I.	INTRODUCTION	1
II.	BACKGROUND	3
	A. CURRENT SMALL SATELLITES	4
	B. ORION HISTORY	8
	C. ORION PRELIMINARY DESIGN	9
III.	SPECIAL THREE-AXIS CONSIDERATIONS	18
	A. ALTERNATE THREE-AXIS SCHEMES	18
	B. FUEL SAVING METHODS	19
	C. SOLAR PANELS	24
IV.	THREE-AXIS ATTITUDE DETERMINATION	26
	A. SATELLITE DYNAMICS	27

B.	EXTERNAL DISTURBANCES	36
1.	Gravity Gradient Torque	36
2.	Aerodynamic Drag Torque	38
C.	SENSORS AND ACTUATORS	41
1.	Horizon Sensors	42
2.	Sun Sensors	44
3.	Magnetometers	45
4.	Rate Gyroscopes	46
5.	Hydrazine Thrusters	48
V.	MINIMUM FUEL-TIME PROBLEM	54
A.	ON-STATION CONTROL LAW	54
B.	LIMIT CYCLE CONTROL	62
C.	ACQUISITION PHASE CONTROL	65
D.	LIMIT CYCLE CONTROL FOR ORION	74
E.	ENVIRONMENTAL DISTURBANCE EFFECTS	80
VI.	SUMMARY AND CONCLUSIONS	92

APPENDIX ATTITUDE CONTROL AND EXTERNAL DISTURBANCE	
PROGRAMS	96
LIST OF REFERENCES	104
INITIAL DISTRIBUTION LIST	106

I. INTRODUCTION

The current ORION design uses spin stabilization, but a truly general purpose satellite should provide attitude control design options for possible payloads. In surveys of likely Navy and Air Force Space Test Program (STP) payloads during the past decade, the majority of the requests were for three-axis stabilization as shown in Table 1-1 [1]. This bears out for the potential customers who have shown an interest in the Orion bus. The intent of this thesis is to investigate a mass expulsion three-axis stabilization design as an ORION bus option.

A three-axis stabilized Orion bus will undoubtedly be more expensive than a spin stabilized version. Limited changes to the original design are desirable. Modified deployable solar panels will be necessary to achieve the required end-of-life power. Additionally, a revised sensor package with more complex sun, horizon sensors and rate gyros will be reviewed. This thesis investigates minimum fuel-time optimization with respect to thruster operation using Pontryagin's Minimization Principle. The effects of external disturbances including gravity gradient and aerodynamic drag cannot be ignored. Models of a three-axis ORION were simulated.

Table 1-1 SUMMARY OF TYPICAL NAVY/STP PAYLOAD REQUIREMENTS [1]

Mass	32 lbm
Volume	2.36 ft ³
Power	34 watts
DataRate	5000 bits/sec
Orbit	200-800 nm circular
Inclination	0°-30° or 60°-120°
Instruments	Particle counter or Lens
Control	3 Axis, $\pm 75^\circ$

II. BACKGROUND

Today most satellites built in Western countries are large, complex and multi-mission/payload capable. The cost of additional payloads has proven exponential due to many factors, of which the most debilitating is that contractors are not motivated to organize their program structures efficiently. Other factors include: expensive launch from only two available sites, the loss incurred when a booster or satellite subsystem fails and the increased testing required before launch. This puts the free world in a highly undesirable position. Reserve assets and the ability to produce large numbers quickly i.e., surge capability for these high value satellites is extremely limited, if not nonexistent. In addition, most programs have been stalled at the 1970-75 technology level due to a general fear of using unproven components when the probability of success is already questionable and the cost is unacceptable. The concept of small, cheap satellites should not work against but with current programs. A multi-site launch capability exists from ships, submarines, aircraft and mobile platforms. New technology can be implemented and space qualified on low value vehicles. The ability to build up reserves and to launch

several satellites at a time becomes viable. The advantages are myriad.

A. CURRENT SMALL SATELLITES

The present U.S. menu of small proven space platforms consists of SPARTAN, NUSAT, GLOMR and LDEF [1]. SPARTAN is a retrievable rectangular platform launched from the Space Shuttle that can fly alongside for only 2.5 days with a payload limit of 1000 pounds. NUSAT (Northern Utah Satellite) is also Shuttle deployed but from a Get-Away-Special (GAS) canister with a specially designed launch mechanism displayed in Figure 2-1.

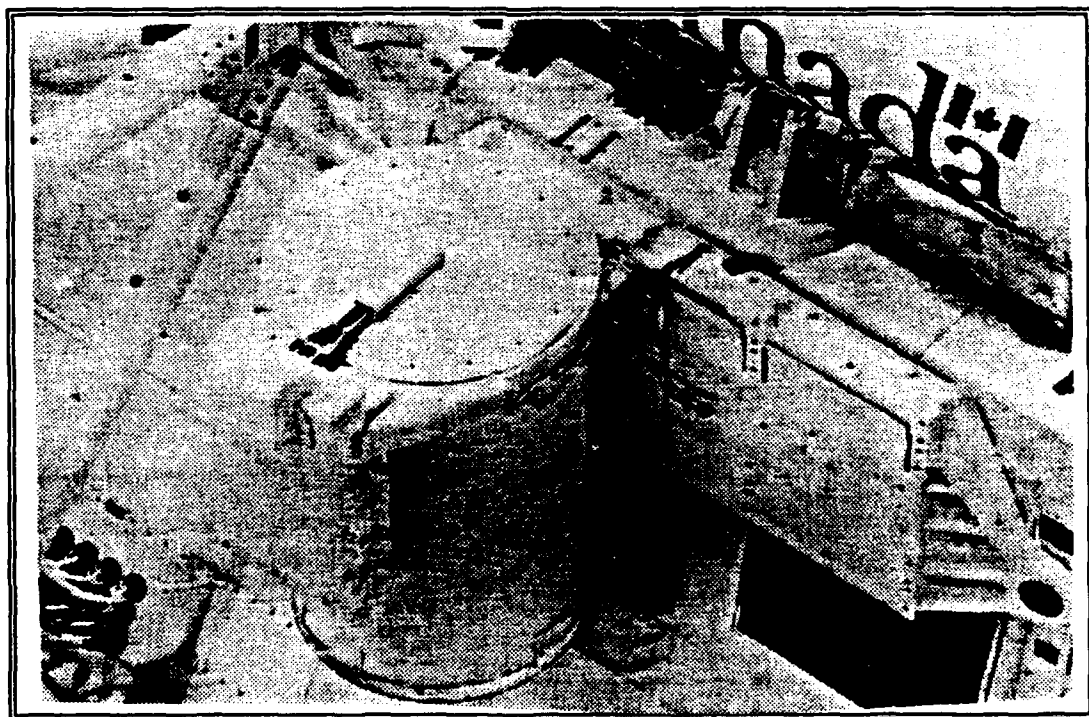


Figure 2-1 Get-Away-Special Canister [1]

GLOMR (Global Message Relay) was a DARPA (Defense Advanced Research Project Agency) payload which used the NUSAT design. LDEF (Long Duration Exposure Facility) is basically a large (up to 20,000 pounds), multi-experiment platform that provides a facility for extended space exposure. Figures 2-2, 2-3 and 2-4 illustrate SPARTAN, NUSAT and GLOMR. Though these represent advancements in small satellite development, they are fundamentally free-flying structures incapable of transfer to higher orbits or long duration attitude control [1].

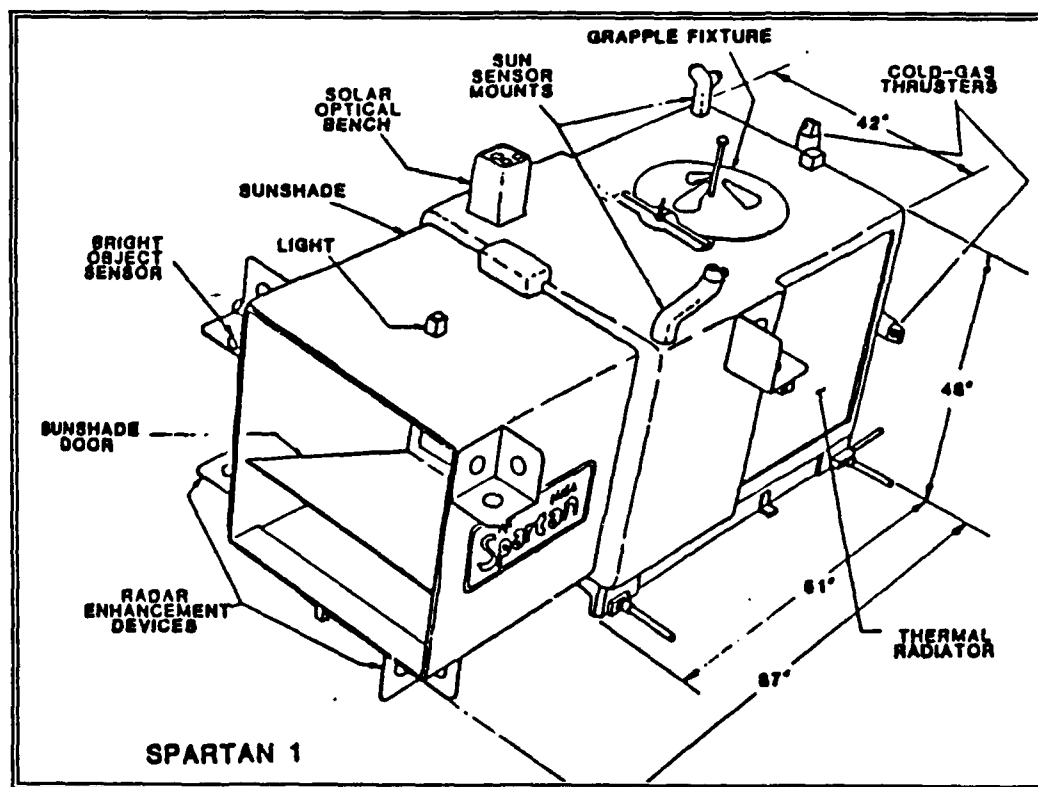


Figure 2-2 Structure for Spartan Spacecraft [1]

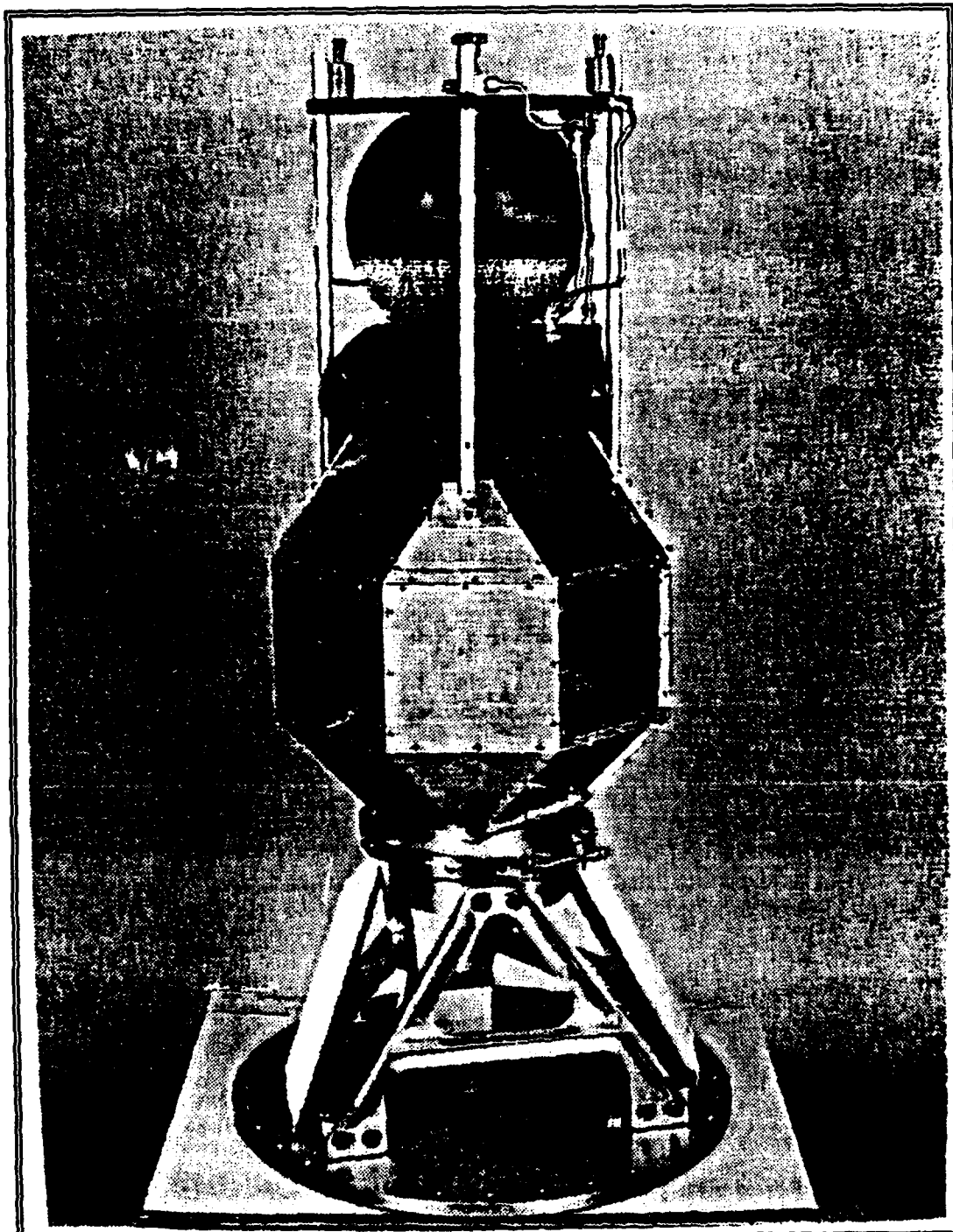


Figure 2-3 Weber State College Second Generation NUSAT [1]

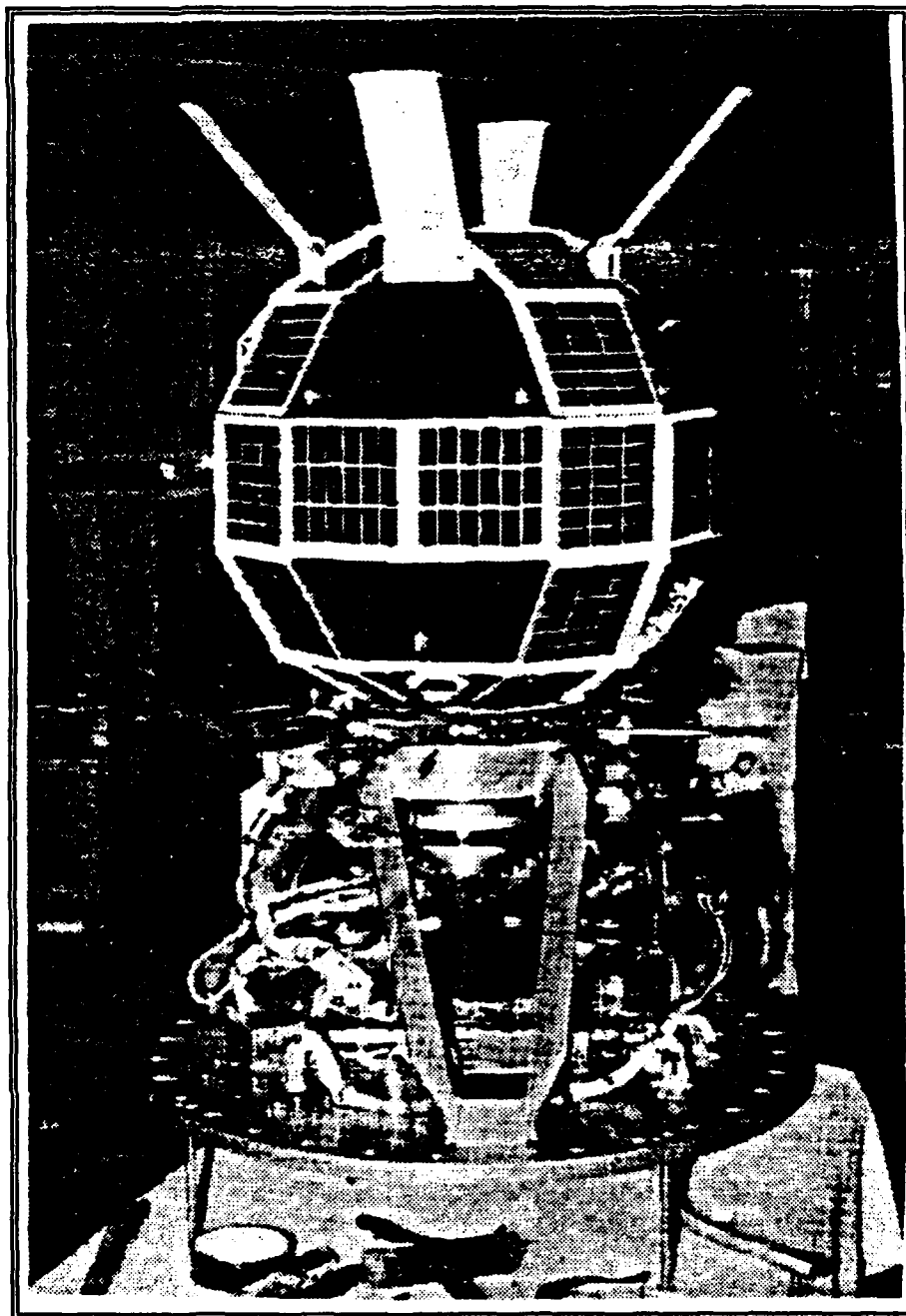


Figure 2-4 DARPA GLOMR Satellite [1]

The ability to produce small multi-purpose satellites has existed since the dawn of the space age. The need to produce a simple yet reliable, low cost satellite bus that is available to commercial and military interests alike has never been as great as it is now. The Naval Postgraduate School (NPS) satellite bus concept not only encompasses propulsion and attitude control subsystems, but also standard electric power, telemetry, thermal and computer subsystems.

B. ORION HISTORY

The history of NPS satellite development began in spring 1985 when the then Chairman of the NPS Space Systems Academic Group, Dr. Allen Fuhs, taught the annual spacecraft design course. The project for that particular class of space engineering and operations students was the design of a small submarine launched satellite [1]. The course was taught two more years before Dr. Fuhs retired from NPS. Each of these two classes worked on applications of the satellite. One student, LCDR Austin Boyd, was so intrigued with the basic concept that he pursued a thesis focused on the simple, reliable design of three satellite subsystems: structure, propulsion and attitude control. LCDR Boyd proposed a Shuttle GAS canister deployable satellite, like GLOMR or NUSAT. The GAS program is a Shuttle option that allows inexpensive, autonomous experiments to fly space available in the cargo bay [1]. Due to the unceasing efforts of LCDR Boyd and Dr.

Fuhs, agencies such as DARPA, SDIO (Strategic Defense Initiative Organization) and Navy/Air Force STP (Space Test Program) Offices began showing a marked interest in the GAS satellite named ORION and in small spacecraft in general. This interest prompted the USAF STP office to pursue the development of an extended and enlarged GAS canister with an improved launch mechanism. The improved GAS can illustrated in Figures 2-5 and 2-6 can hold a satellite that is 35 inches long, 19 inches in diameter and can weigh up to 250 pounds [1]. In addition to the NPS satellite, three other efforts were launched in 1986 toward small, general purpose design. These included: "T-SAT" by INTRASPACE Company, an advanced NUSAT by GLOBESAT and American Rocket Company and an Orion type design by TRW [1]. This sudden flurry of activity in the small satellite business was capped by an encouraging DARPA program initiated in early 1988 called Lightsat. The Lightsat program promotes low-cost, lightweight satellites to be utilized by operational field commanders [1]. It appears that the idea of the small, general purpose satellite has finally come of age.

C. ORION PRELIMINARY DESIGN

The preliminary design of ORION adopted by LCDR Boyd is simple, reliable and relatively inexpensive with a price tag of about \$1.5 million. "A general purpose architecture was defined as the ability to successfully integrate various

payloads of the proper size while providing a propulsion, attitude control and standardized electrical, data and attitude control interfaces." [1]

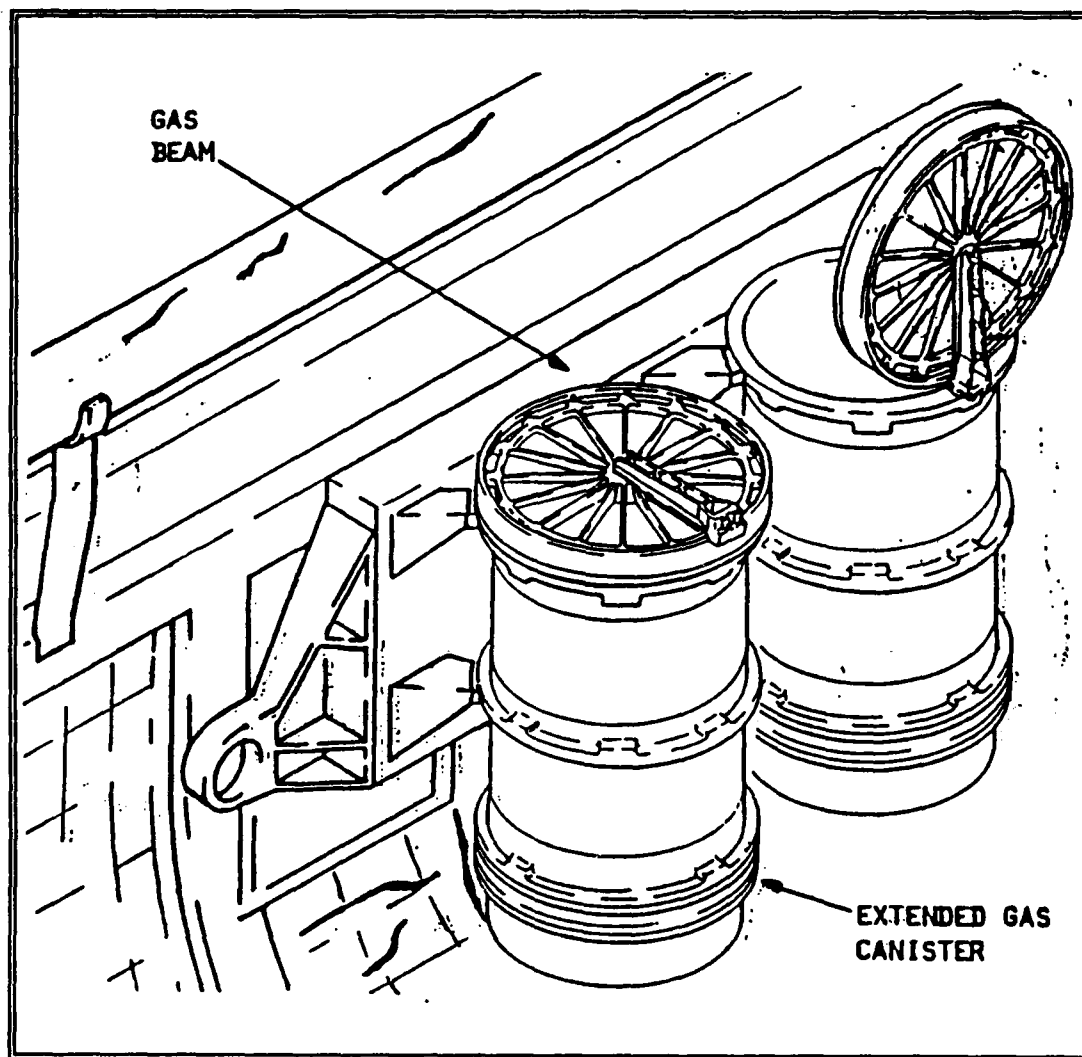


Figure 2-5 USAF/BALL Aerospace Extended GAS Canister [1]

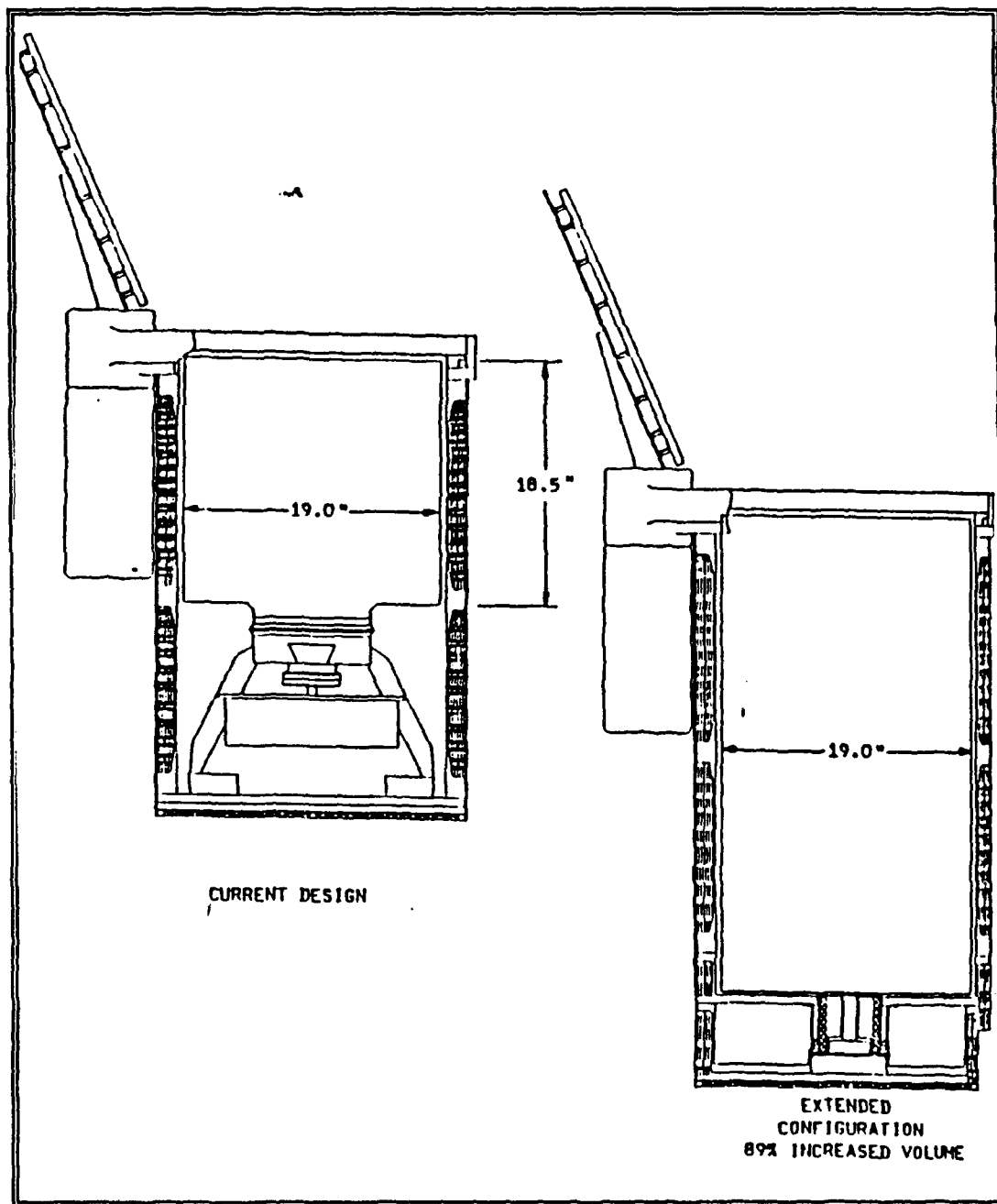


Figure 2-6 Comparison of GAS Canister Design [1]

General purpose naturally implies that trade-offs must be made in the design of the payload in order to reap the benefits of a low cost bus. Trade-offs are weight and size driven. The payload of any generic bus is constrained to weight and volume limits that do not affect most designs where the bus is built around the payload. A brief description of ORION subsystems will allow insight into the preliminary design.

The ORION structural subsystem weighs approximately 40 lbm and consists of a .62" thick baseplate, three .75" honeycombed equipment decks, four extruded 1/16" thick longerons which house 78.5" long booms, a 1" thick honeycombed propellant tank strongback and four .05" thick semicircular skin panels. The baseplate, longerons, booms and skin panels are made of 7075-T6 aluminum while the honeycombed items use stainless steel facing material. The booms are designed to support magnetometers or 2 lbm tip weights to provide stability about the longitudinal spin axis. During Shuttle launch, this cylindrical structure will experience less than .035" of deflection. In compliance with NHB 1700.7A safety specifications, the ORION model resonates above 35 Hz at modes of 160.8, 178.3 and 244.6 Hz [1]. Figure 2-7 demonstrates the basic structural subsystem.

The propulsion subsystem uses hydrazine monopropellant and Shell 405 catalyst. The hydrazine tank is a spherical

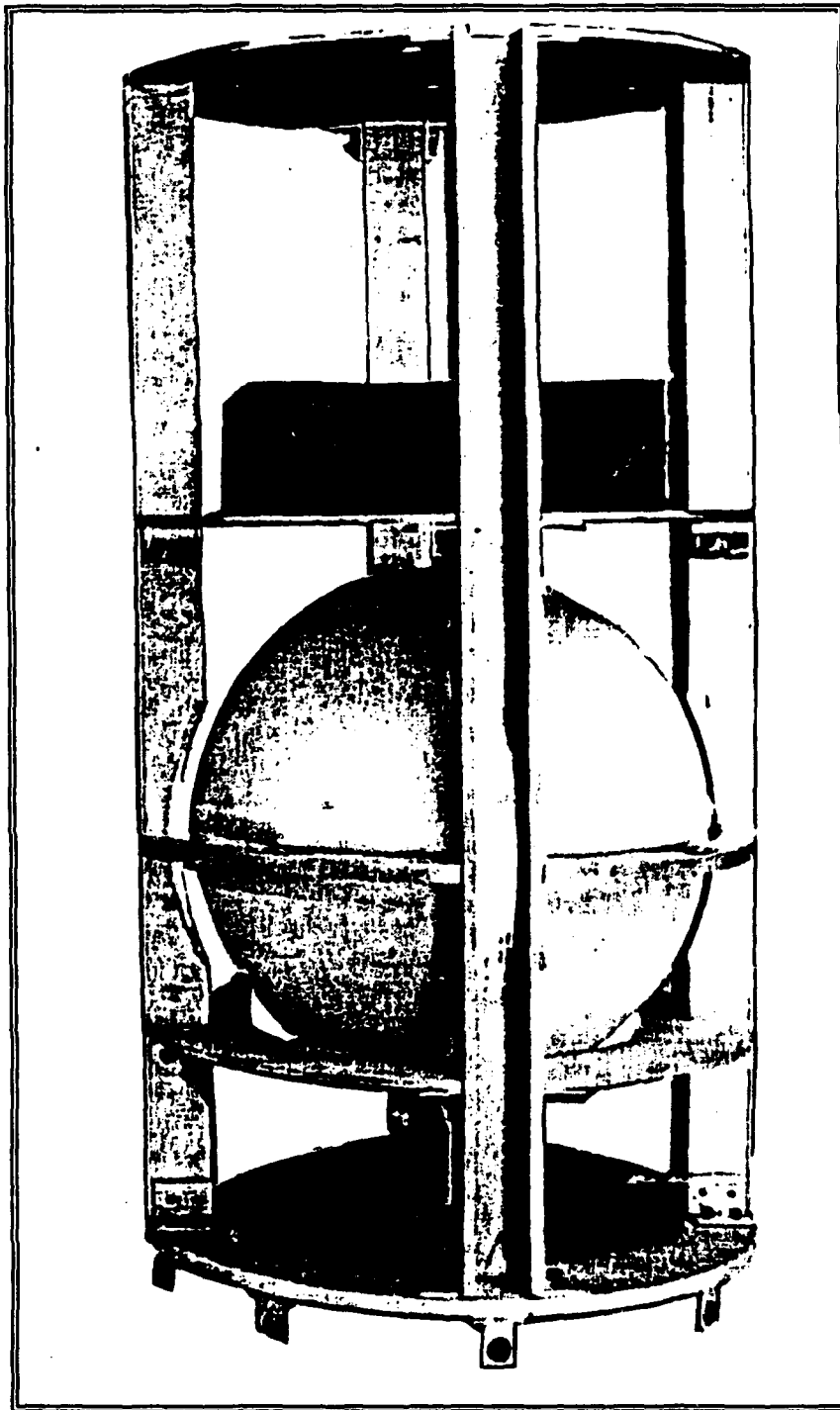


Figure 2-7 ORION Structural Mock-up [1]

positive expulsion type. It is nitrogen pressurized and can hold up to 71.5 lbm of monopropellant. One 40 lbf thruster will be used for orbital maneuvers while six 0.1 lbf thrusters will be used for attitude control [1]. Design requirements included the ability to transfer from a Shuttle orbit of 135 nm to 835 nm, the lower limit of the Van Allen radiation belts, in addition to a lifetime expectancy of 90 days to 3 years [1].

The ORION power subsystem consists of 1765 in² of the outer skin covered by solar cells and a back-up supply of 24 NiCad cells rated at 1.25 volts each [1]. An end-of-life DC requirement of 60 watts is based on the following assumptions: (1) one third of the skin surface area will be exposed to the sun, (2) solar cell efficiency of 14%, (3) solar constant of 125.6 watts/ft² and, (4) 10% degradation per year. Even with these liberal assumptions, end-of-life power occurs after only 18 months.

The ORION attitude control subsystem consists of six 0.1 lbf thrusters, one sun sensor, one horizon sensor and four magnetometers mounted on 78.5" booms. Spin stabilization about the longitudinal axis with ± 1 degree of pointing accuracy was chosen as the simplest, most cost effective attitude control design option for ORION [1]. The fuel budget of the attitude control subsystem is limited by transfer altitude and effective deployment of the stabilizing booms in

this configuration. Figure 2-8 describes the attitude control and propulsion subsystems.

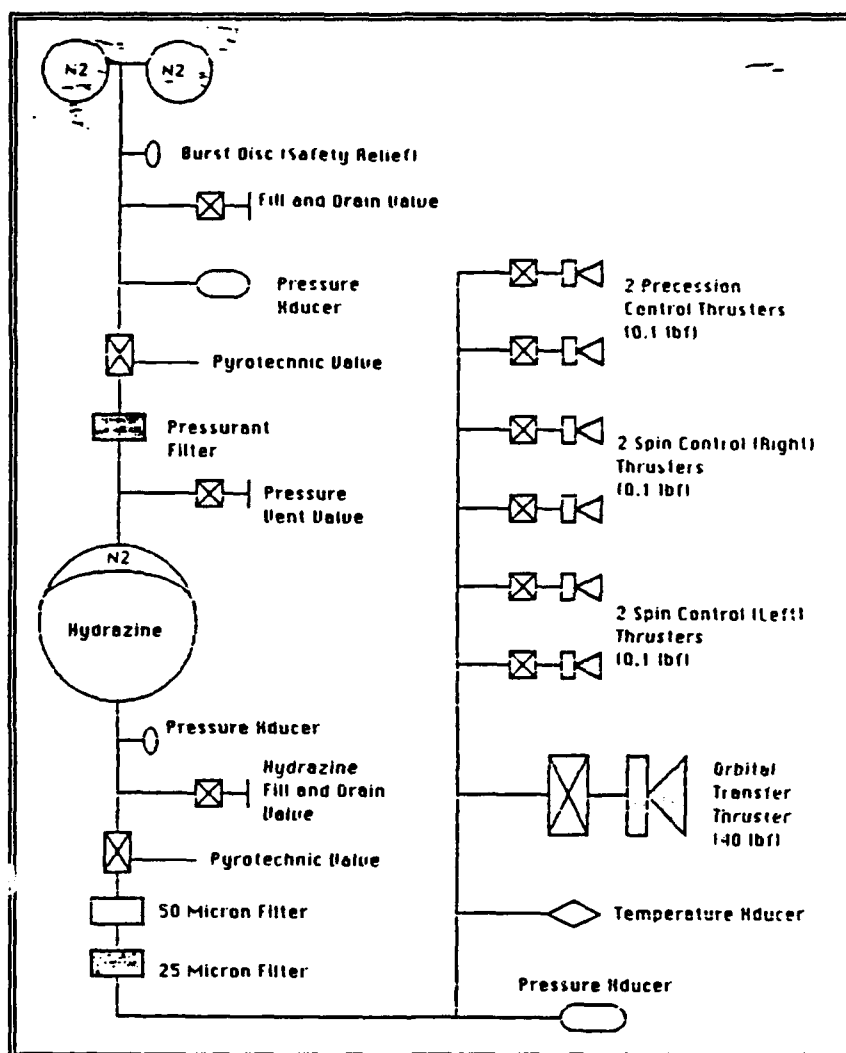


Figure 2-8 ORION Propulsion and Attitude Control Subsystems [1]

The remaining ORION subsystems were briefly discussed by LCDR Boyd. The thermal control subsystem consists of strip heaters and insulating blankets. The health and welfare of Orion will be monitored by a computer subsystem and telemetry link [1]. Note that the preliminary design assumes Space Shuttle deployment which is questionable due to the as yet approved use of hydrazine in a GAS can. After all the subsystem masses are tallied, a total of about 32 lbm remains for payload usage. Figure 2-9 shows the component placement for the ORION preliminary design.

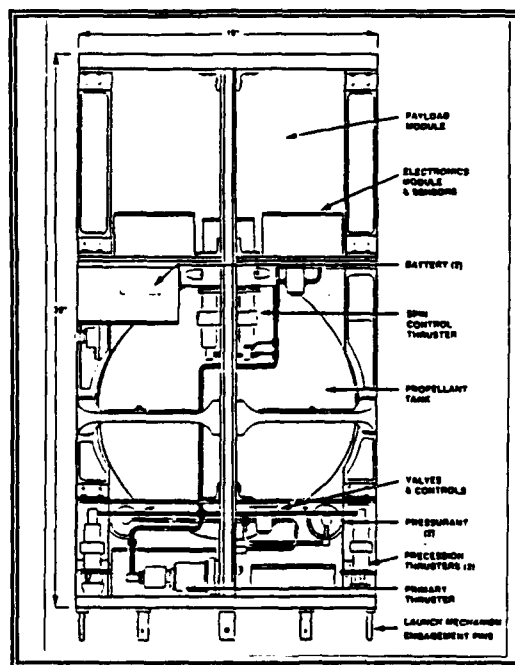


Figure 2-9 ORION Cross-section [1]

Table 2-1 ORION COMPONENT MASSES [1]

Component	Mass(lbm)
Top plate	1.65
Longerons(4)	5.80
Payload Midplate	1.65
Propellant Tank Strongback	4.20
Baseplate	9.75
Launch Restraint Pins(8)	.80
Pressurant Mid-deck	1.05
Batteries/Boxes(4)	28.0
Earth Sensor	.30
Propellant Tank	13.0
Hydrazine Control Thrusters(6)	9.18
Orbital Transfer Thruster	1.93
Attitude Control and Payload Computer	16.0
Telemetry Transmitter/Receiver(2)	10.0
Pressurant Gas and Bottle(2)	5.00
Fill and Drain Valve(3)	2.10
Assorted Propulsion Tubing	2.00
Pyrotechnic Valve(2)	1.00
Power Conditioning Circuits(2)	4.00
Payload	32.0
Skin and Fasteners	12.0
Solar Cells	.70
Booms(4)	4.20
Hydrazine Fuel	71.5
Magnetometers(4)	2.00
Total Mass	245.81

III. SPECIAL THREE-AXIS CONSIDERATIONS

A three-axis stabilized ORION will impose additional constraints on the structural, propulsion and power subsystem design compared to a spin stabilized version. A major consideration is the increased fuel usage for a mass expulsion attitude control system (ACS). There are several options available to extend the ORION lifetime. Although not discussed in this thesis, but promoted as avenues of further research, there exist other energy efficient three-axis attitude control schemes. [2]

A. ALTERNATE THREE-AXIS SCHEMES

Momentum bias systems consist of a momentum wheel and either mass expulsion thrusters or magnetic torquers to dump excess momentum and control motion about the other two axes. The momentum wheel supplies gyroscopic stiffness which, in essence, cancels unwanted moments about one axis. Significant fuel savings result in the thruster moment bias design in comparison to the all-thruster system, but the added mass of the wheel must be compensated to maintain the same payload mass. Magnetic torquers use the torque produced when a magnetic dipole cuts through the Earth's magnetic field, but they are limited to low Earth orbits. They provide an endless

reservoir of control energy as long as current flows in the satellite magnets, but they are not preferred if fast reaction times are required. The necessity for propellant is diminished unless orbital transfer is desired. [2]

Gravity gradient boom and thrusters or magnetic torquers afford a less expensive form of control since the boom is passive. Accuracy is reduced compared to the active momentum bias system, but fuel is still conserved.

Reaction wheel systems operate independently about each axis just as a three-axis mass expulsion system does. [2] Thrusters are employed to dump excess wheel momentum so a fuel savings is realized when equated to the all-thruster system. The disadvantages of reaction wheel systems include the increased weight, complexity and cost of three wheels which could disqualify this system for a small satellite of ORION caliber.

B. FUEL SAVING METHODS

In addition to the minimum fuel-time control laws discussed and simulated in Chapters V and VI, fuel conservation can be practiced by restricting the employment of the 40 lbf orbital insertion thruster. Confining usage of the 40 lbf thruster to negation of the effects of aerodynamic drag could liberate most of the hydrazine for on-station attitude control.

The ability to transfer between circular orbits is a luxury for a small satellite, but ΔV required is lessened when the booster that carries ORION can insert close to the requested altitude. The original ORION designers assumed that the Space Shuttle would be the only practical launch option. In light of the stringent safety requirements for a man-rated payload, the shuttle seems to be the least feasible launch alternative when dealing with hydrazine monopropellant. Table 3-1 lists current launch vehicles, payload weights, altitude and launch costs [6].

Table 3-1 SMALL SATELLITE BOOSTER OPTIONS

Booster Name	Payload(kg)	Altitude(km)	Cost(10^6)
Titan	14,030	LEO	\$90+
	4525	GEO	
Atlas/Centaur	5882-7625	LEO($i=28.5^\circ$)	\$40
	2330-3145	GTO($i=28.5^\circ$)	
Delta II	4460	LEO	\$35-50
	1891	GTO	
Scout G-1	219	555	\$11-12
*Minuteman III	680	LEO(polar)	\$5
*Conestoga II	724	LEO($i=98^\circ$)	\$7.03
	1040	LEO($i=38^\circ$)	
*Super Starbird	2080	LEO($i=0^\circ$)	\$6+
	724	LEO(polar)	
Liberty 1A	7260	LEO	\$2-4
Pegasus	407	LEO($i=0^\circ$)	\$6
	271	LEO(polar)	
<u>Foreign Systems</u>			
Ariane IV(France)	4200	GTO	\$80+
Long March(China)	1267-2489	LEO	\$35+
	271-1358	GTO	
*H-2(Japan)	8978	LEO	?
	1990	GEO	
Proton(USSR)	20,000	LEO($i=52^\circ$)	\$25-40
	2000	GEO	

*not commercially available yet

If ORION must transfer to a higher orbit, the fuel budget will be driven by the ΔV required. The equation for the velocity of a circular orbit is

$$V_c = (\mu/R)^{1/2} \quad (3.1)$$

where $\mu=GM_e=3.986 \times 10^5 \text{ km}^3/\text{s}^2$, G is the Universal gravitational constant and M_e is Earth's mass. The radius $R=R_e+h$, $R_e=6378 \text{ km}$ is Earth's radius and h is the satellite altitude. A Hohman transfer is the most efficient means of transitioning between coplanar orbits and is depicted in Figure 3-1.

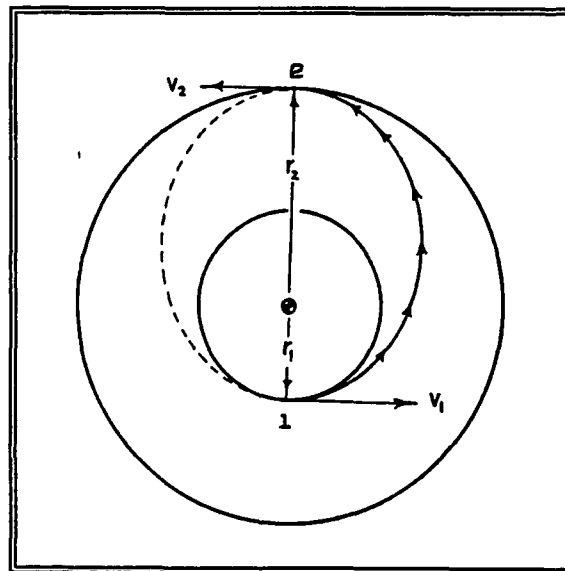


Figure 3-1 Hohman Transfer [4]

The total ΔV required for a Hohman transfer is

$$\begin{aligned} \Delta V_1 &= V_1 - V_{c1} \\ \Delta V_2 &= V_{c2} - V_2 \\ \Delta V_T &= \Delta V_1 + \Delta V_2 \end{aligned} \quad (3.2)$$

where ΔV_1 is the difference between the elliptical transfer orbit velocity at perigee and the inner circular orbit velocity and ΔV_2 is the difference between the transfer orbit velocity at apogee and the desired circular orbit velocity. The elliptical orbit transfer velocity is

$$V = ((2\mu/R) + E)^{1/2} \quad (3.3)$$

The specific mechanical energy of the transfer orbit is

$$E = - \mu/2a \quad (3.4)$$

where a is the length of the semi-major axis of the transfer ellipse. The thrust equation for a rocket engine is

$$F = m_e V_e + A_e (p_e - p_o) \quad (3.5)$$

m_e = mass flow rate
 V_e = exhaust velocity
 A_e = exhaust cross-section
 p_e = exhaust pressure
 p_o = ambient pressure

Specific impulse is a performance measure of the thrust to mass flow rate ratio for a rocket

$$ISP = F/\dot{m} \quad (3.6)$$

ISP is a function of propellant type. The specific impulse of hydrazine is $ISP=235$ sec. The total impulse is the aggregate thrust obtained over time

$$I_T = \int_t F dt = ISP m_p \quad (3.7)$$

where m_p is propellant mass. The total propellant mass required to boost a satellite to a higher orbit using a Hohman transfer is

$$m_p = m_o (1 - e^{(-\Delta V / ISP_g)}) \quad (3.8)$$

where m_o is the original satellite mass. The curves in Figure 3-2 demonstrate the propellant mass required to boost ORION.

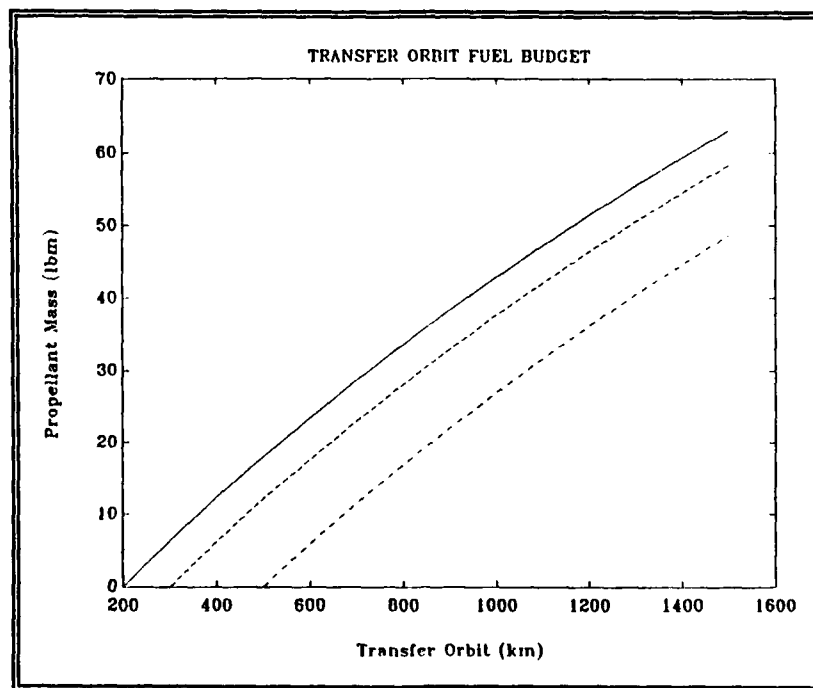


Figure 3-2 Hydrazine Required by ORION for Transfer Orbits

ORION will only carry 71.4 lbm of hydrazine so the fuel remaining after transfer is allotted for attitude control. [1]

C. SOLAR PANELS

Three-axis stabilized satellite power subsystems generally include arrays of solar panels that extend after the transfer orbit. Panels allow more direct utilization of the sun's energy by maximizing the perpendicular rays of received sunlight through proper panel rotation. Solar cell output voltage is optimized in this configuration. This is the topic of another thesis design study and will not be examined in detail in this or later chapters. Solar panels will add more mass to the ORION structure and thereby add further size constraints to other subsystems. Suggested solar array designs for a three-axis ORION consist of cylindrical body mounted arrays that deploy or accordion style arrays that unfold and extend as shown in Figures 3-3 and 3-4.

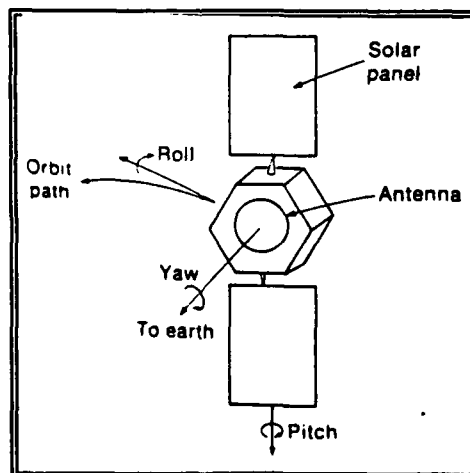


Figure 3-3 Extended Body Mounted Solar Array [5]

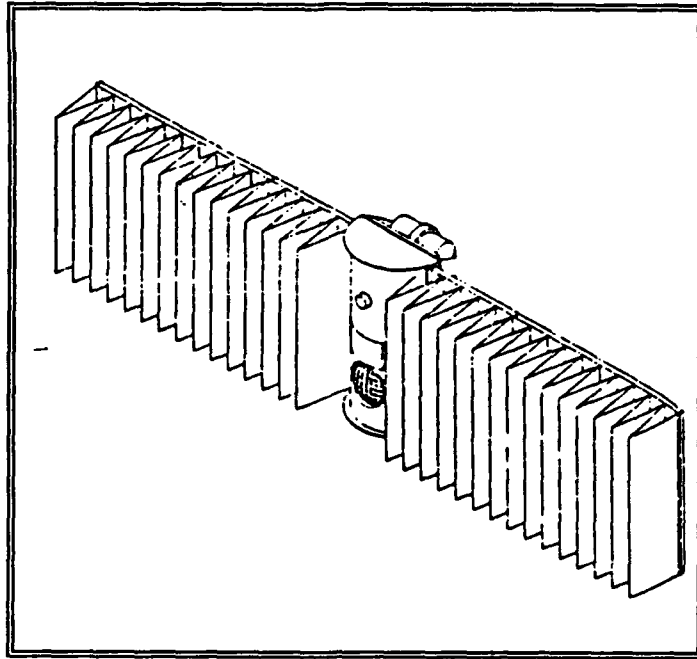


Figure 3-4 Accordion Solar Arrays [1]

Solar panels alter the moments of inertia of a satellite when deployed. ORION attitude control design assumes that $I_x = I_z$ which greatly simplifies the control problem by causing one axis to act independently of the other two in all regimes of motion. For $I_x \neq I_y \neq I_z$, coupling occurs between all axes when the angular rate errors are large. An axially symmetric array would alleviate the coupling in one axis.

The additional constraints on fuel and power budgets levied by a three-axis satellite are not insurmountable, but they must be investigated in more detail in future ORION design analyses.

IV. THREE-AXIS ATTITUDE DETERMINATION

Satellite attitude control systems (ACS) consist of angular position and rate sensors or estimators and control actuators as shown in Figure 4-1. The sensors and estimators feed back angle and angle rate information in the form of error signals to be processed as required through a programmed control law. The actuators then react to commands from the ground or on-board microprocessors to implement corrections in attitude. The satellite is affected by unwanted internal and external torques such as gravity gradient, aerodynamic drag and thruster misalignment. An ACS conforms to the equations of motion and reacts to known and unknown disturbances. [2]

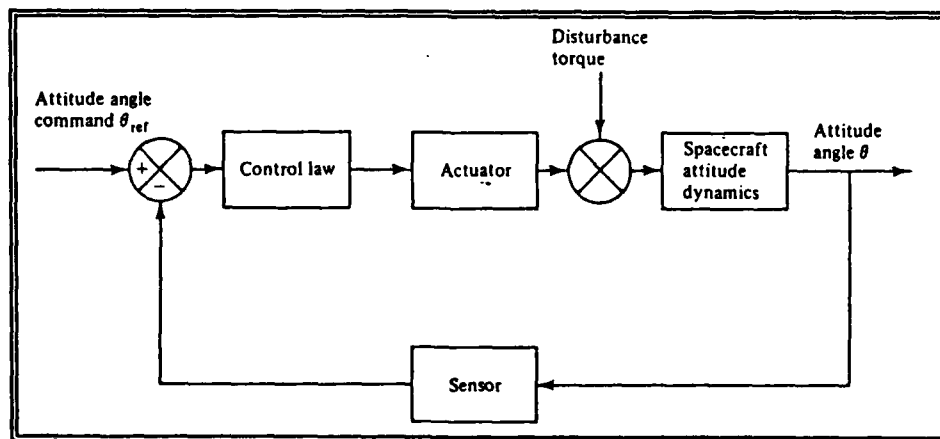


Figure 4-1 Attitude Control Block Diagram [2]

A. SATELLITE DYNAMICS

In modeling the ORION ACS, rigid-body dynamics will be assumed. Rigid body dynamics are used to approximate systems that have limited flexibility. The equations of motion for a satellite can be described by the movements of a point mass in space as shown in Figure 4-2.

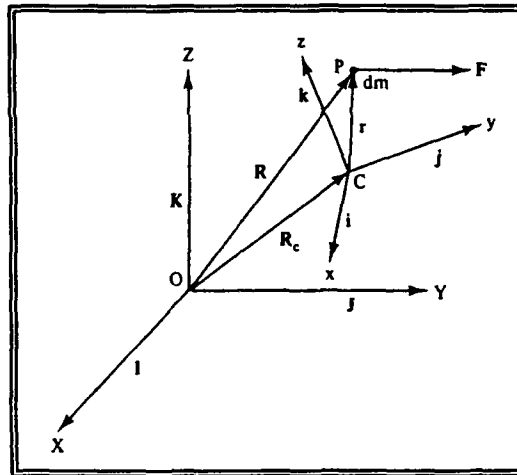


Figure 4-2 Motion of a Point Mass [2]

The mass P can experience rotation or translation with respect to the inertial reference frame XYZ. The position vector of P is

$$R = R_c + r \quad (4.1)$$

where R_c is a vector from the XYZ inertial frame to the xyz body frame and r is the position vector of P in the xyz frame.

$$r = xi + yj + zk \quad (4.2)$$

The absolute velocity of P is

$$\mathbf{V} = \dot{\mathbf{R}} = \dot{\mathbf{R}}_c + \dot{\mathbf{r}} \quad (4.3)$$

where $\dot{\mathbf{r}}$ includes linear and angular velocity in the body frame.

$$\dot{\mathbf{r}} = \dot{\mathbf{r}}_{rel} + \boldsymbol{\omega} \times \mathbf{r} \quad (4.4)$$

Substituting (4.4) into (4.3), the absolute velocity becomes

$$\mathbf{V} = \mathbf{V}_c + \mathbf{V}_{rel} + \boldsymbol{\omega} \times \mathbf{r} \quad (4.5)$$

The absolute acceleration of P is the derivative of absolute velocity.

$$\mathbf{a} = \mathbf{a}_c + \mathbf{a}_{rel} + 2\boldsymbol{\omega} \times \mathbf{V}_{rel} + \boldsymbol{\omega} \times (\boldsymbol{\omega} \times \mathbf{r}) \quad (4.6)$$

In order to simplify future equations, two assumptions will be made. The xyz frame is internal to the spacecraft body so that $\mathbf{V}_{rel}=0$ and the spacecraft center of mass (CM) coincides with the center of the body frame so that $\int_m \mathbf{r} dm = 0$. The linear momentum of a rigid-body is defined as the integral of the absolute velocity times the differential mass.

$$\mathbf{P} = \int_m (\mathbf{V}_c + \boldsymbol{\omega} \times \mathbf{r}) dm = m\mathbf{V}_c \quad (4.7)$$

Angular momentum of a rigid-body is defined as the moment of the linear momentum or the cross product of \mathbf{r} and \mathbf{P} .

$$\mathbf{H}_c = \int_m (\mathbf{r} \times \mathbf{V}) dm = \int_m \mathbf{r} \times (\boldsymbol{\omega} \times \mathbf{r}) dm \quad (4.8)$$

The angular velocity vector is equal to

$$\boldsymbol{\omega} = \omega_x \mathbf{i} + \omega_y \mathbf{j} + \omega_z \mathbf{k} \quad (4.9)$$

Moments and products of inertia are analogous to the mass of a linear system but relate to mass distribution for a rotating rigid body. Inertia is the sum of the products of the component masses and their distance from the chosen axis of rotation.

$$I = \sum m_i r_i^2 \quad (4.10)$$

Moments of inertia become

$$I_x = \sum m_i (y^2 + z^2) \quad (4.11)$$

$$I_y = \sum m_i (x^2 + z^2)$$

$$I_z = \sum m_i (x^2 + y^2)$$

Figure 4-3 shows ORION fuel and dry mass densities along the X and Y axes.

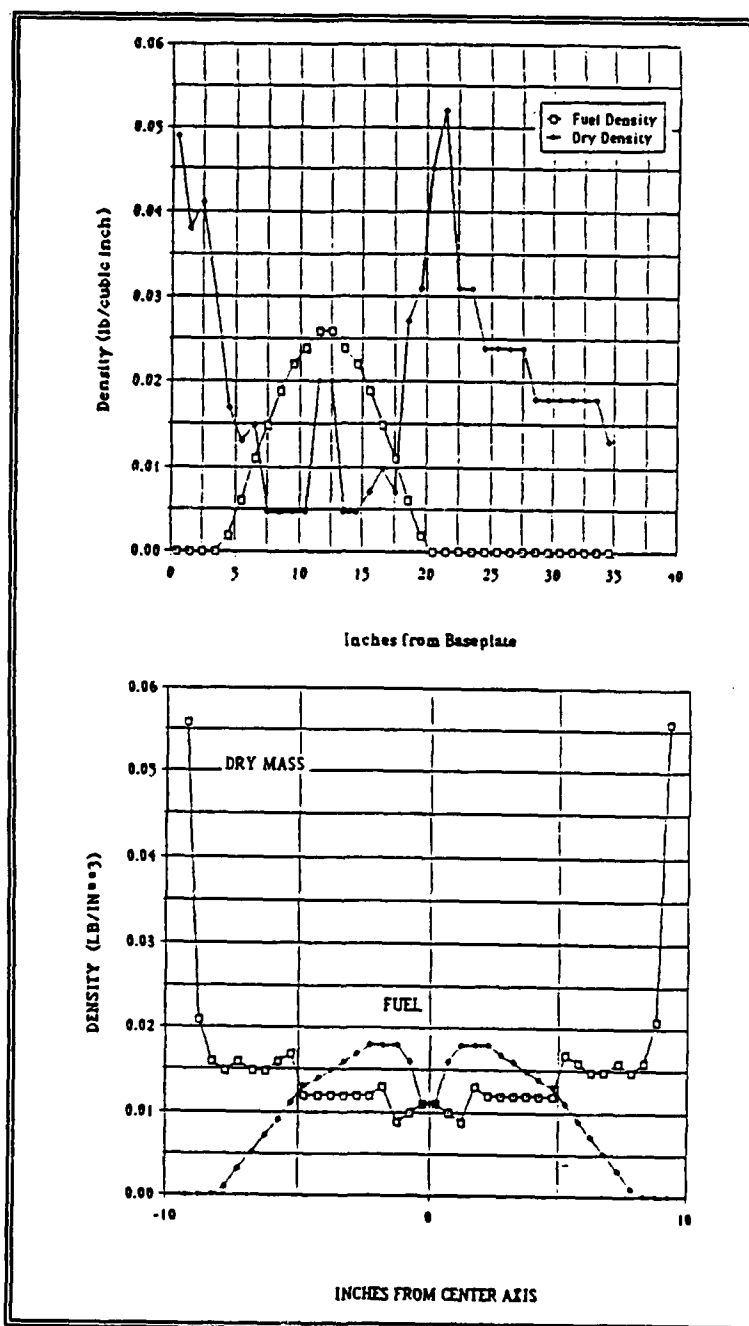


Figure 4-3 Mass Distribution a) X-axis
b) Y-axis [1]

Table 4-1 lists preliminary subsystem masses and principal moments of inertia for ORION.

Table 4-1 SUBSYSTEM MOMENTS OF INERTIA [12]

Subsystem	Mass(kg)	I _x	I _y	I _z
Structure	28.99	2.4652	2.4652	1.4148
Propulsion	44.57	1.6218	1.6647	0.8844
Telemetry	4.61	0.6089	0.5500	0.0652
Attitude Control	4.41	9.3621	9.3827	18.6291
Computer	3.45	0.3482	0.3482	0.0214
Electrical Power	13.84	0.7379	0.5016	0.3011
Thermal	0.0	0.0000	0.0000	0.0000
Payload	11.22	1.0812	1.1117	0.0916
Total (kg-m ²)	111.09	16.23	16.02	21.04
Total (Slug-ft ²)	7.61	11.9	11.82	15.97
Without booms				
Total (kg-m ²)	106.68	6.8633	6.6415	2.7758
Total (Slug-ft ²)	7.31	5.06	4.90	2.05

The products of inertia below are zero when the principal moments of inertia are chosen as rotation axes.

$$I_{xy} = \sum m_i xy$$

$$I_{xz} = \sum m_i xz$$

$$I_{yz} = \sum m_i yz$$

After solving (4.8) and recognizing (4.9) and (4.11), the angular momentum becomes

$$H_c = \begin{bmatrix} I_x & -I_{xy} & -I_{xz} \\ -I_{xy} & I_y & -I_{yz} \\ -I_{xz} & -I_{yz} & I_z \end{bmatrix} \begin{bmatrix} \omega_x \\ \omega_y \\ \omega_z \end{bmatrix} \quad (4.12)$$

The inertia matrix is called the inertia tensor. To simplify the design of ORION, the inertia tensor will be assumed diagonal with zero cross terms.

The kinetic energy of a rigid body is defined as the integral of the dot product of the absolute velocity.

$$T = \frac{1}{2} \int_m \mathbf{V} \cdot \mathbf{V} \, dm \quad (4.13)$$

This thesis will focus on rotation only. Substituting (4.5) into (4.13) the kinetic energy reduces to

$$T = \frac{1}{2} \begin{bmatrix} \omega_x & \omega_y & \omega_z \end{bmatrix} \begin{bmatrix} I_x & 0 & 0 \\ 0 & I_y & 0 \\ 0 & 0 & I_z \end{bmatrix} \begin{bmatrix} \omega_x \\ \omega_y \\ \omega_z \end{bmatrix} \quad (4.14)$$

Newton's Second Law can be applied to a rigid body as

$$\mathbf{F} = \int_m \mathbf{a} \, dm = m \mathbf{a}_c \quad (4.15)$$

A moment about the satellite CM is the cross product of distance and force.

$$\begin{aligned} \mathbf{M}_c &= \dot{\mathbf{H}}_c + \int_m \dot{\mathbf{R}}_c \times \dot{\mathbf{r}} \, dm = \dot{\mathbf{H}}_c \\ &= \dot{\mathbf{H}}_{c\text{rel}} + \boldsymbol{\omega} \times \mathbf{H}_c \end{aligned} \quad (4.16)$$

Angular momentum in the body frame can be expressed as

$$H_c = H_x i + H_y j + H_z k \quad (4.17)$$

where xyz coincides with the principal moments of inertia. From (4.12), the elements of the angular momentum vector are

$$H_x = I_x \omega_x \quad (4.18)$$

$$H_y = I_y \omega_y$$

$$H_z = I_z \omega_z$$

After some manipulation, (4.16) is transformed into the Euler Moment equations.

$$M_x = I_x \dot{\omega}_x + \omega_y \omega_z (I_z - I_y) \quad (4.19)$$

$$M_y = I_y \dot{\omega}_y + \omega_x \omega_z (I_x - I_z)$$

$$M_z = I_z \dot{\omega}_z + \omega_x \omega_y (I_y - I_x)$$

Equation (4.19) will be used extensively through out this thesis to simulate ORION attitude control.

An inertial coordinate system with $X_0 Y_0 Z_0$ fixed at the center of the Earth as shown in Figure 4-4 is used as a reference frame when describing satellite motion. The roll axis, X, describes the orbital velocity vector with magnitude, ω_0 , which is assumed constant for a nearly circular orbit. The yaw axis, Z, extends from the satellite CM toward the

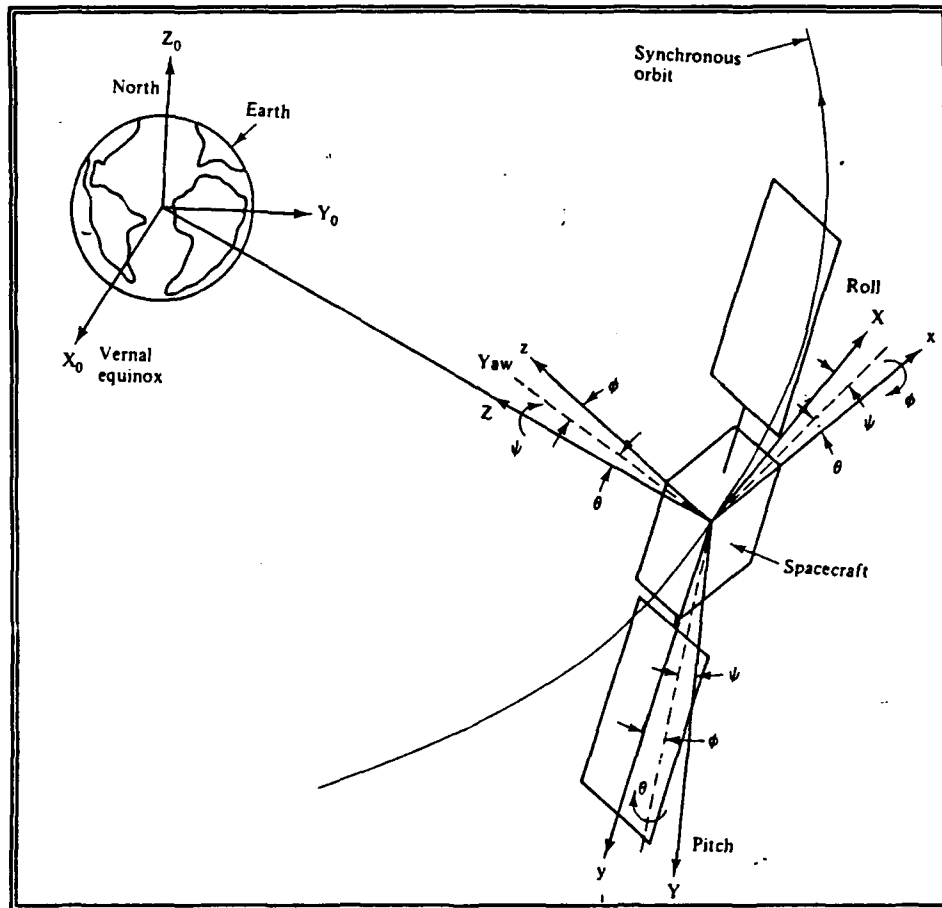


Figure 4-4 Spacecraft Coordinate System [2]

Earth CM. The pitch axis, Y , is perpendicular to the orbital or XY plane. Errors caused by disturbance torques are described by the angles ϕ , ψ and θ about the roll, yaw and pitch axes, respectively. In unperturbed form, the Euler moment equations become

$$\begin{aligned} I_x \dot{\omega}_x &= (I_x - I_z) \omega_y \omega_z \\ I_y \dot{\omega}_y &= (I_z - I_x) \omega_x \omega_z \\ I_z \dot{\omega}_z &= (I_x - I_y) \omega_x \omega_y \end{aligned} \quad (4.20)$$

The right hand side of (4.20) exhibits the coupling that occurs when angular error rates are large. For on orbit control of a three-axis stabilized system the angular velocities are assumed small which reduces (4.20) to

$$\begin{aligned} I_x \dot{\omega}_x &= 0 \\ I_y \dot{\omega}_y &= 0 \\ I_z \dot{\omega}_z &= 0 \end{aligned} \tag{4.21}$$

Satellite acquisition is a stage in which initial large attitude adjustments are made to correct for booster separation. In this phase the satellite frequently experiences a tumbling motion which translates to large errors in angular position and rate. Excess rates must be negated before the on orbit control law can be implemented. Angular velocity errors as viewed from the inertial frame can be expressed as

$$\begin{aligned} \omega_x &= \dot{\phi} - \omega_o \psi \\ \omega_y &= \dot{\theta} - \omega_o \\ \omega_z &= \dot{\psi} + \omega_o \phi \end{aligned} \tag{4.22}$$

Replacing rate errors in the Euler moment equations yields

$$\begin{aligned}
M_x &= I_x(\ddot{\phi} - \dot{\omega}_o\dot{\psi}) + (I_z - I_y)\omega_o(\dot{\psi} + \omega_o\phi) \\
M_y &= I_y \ddot{\theta} \\
M_z &= I_z(\ddot{\psi} + \dot{\omega}_o\dot{\phi}) + (I_y - I_x)\omega_o(\dot{\phi} - \omega_o\psi)
\end{aligned} \tag{4.23}$$

B. EXTERNAL DISTURBANCES

The major external disturbances for low altitude orbits are caused by the Earth's gravitational field and aerodynamic drag. Solar pressure contributions are considered negligible at low altitude but a dominant factor beyond geosynchronous altitudes.

1. Gravity Gradient Torque

Gravity gradient torques can be used as a passive form of three-axis stabilization for Earth pointing payloads if a boom is attached to the satellite. This torque results from the interaction between the earth-satellite masses. [2] The gravitational moment can be expressed as

$$M_G = \int_m \mathbf{r} \times \mathbf{F} \, dm \tag{4.24}$$

where the gravitational force is

$$\mathbf{F} = \frac{\mu(R_e - \mathbf{r})}{R_e^3} dm \left(1 + \frac{3\mathbf{r} \cdot \mathbf{R}_e}{R_e^2} \right) \tag{4.25}$$

Substituting (4.24) into (4.23) results in

$$M_G = \frac{3\mu}{R_e^5} \int (\mathbf{r} \times \mathbf{R}_e) (\mathbf{r} \cdot \mathbf{R}_e) \quad (4.26)$$

where \mathbf{R}_e , the vector between Earth-satellite centers of mass as shown in Figure 4-5 is expressed in the satellite body frame as

$$\mathbf{R}_e = R_e(-\sin\theta \mathbf{i} + \sin\phi \cos\theta \mathbf{j} + \cos\phi \cos\theta \mathbf{k}) \quad (4.27)$$

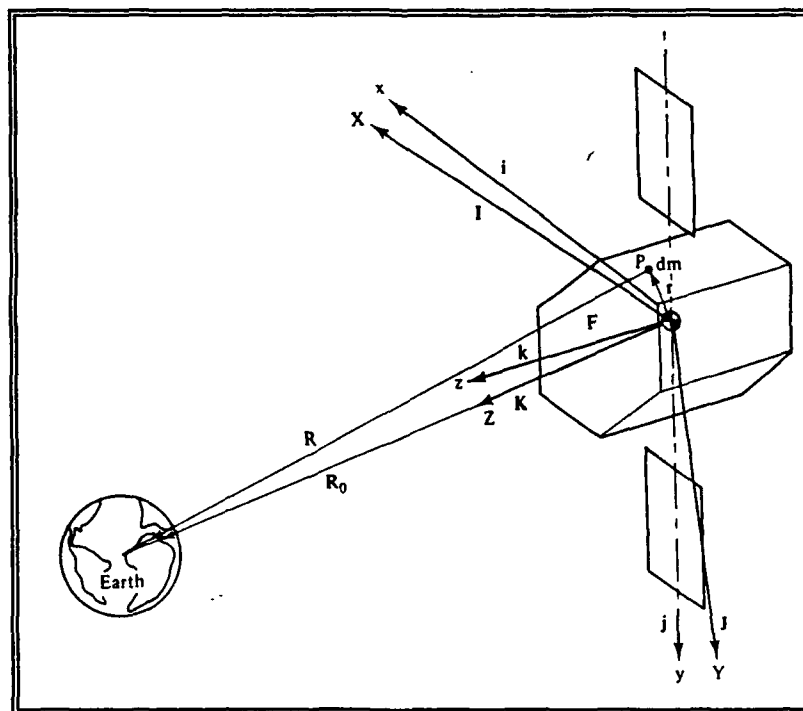


Figure 4-5 Gravity Gradient Moment on a Satellite [2]

For small angle corrections equation (4.26) reduces to

$$\mathbf{M}_G \approx \begin{Bmatrix} \phi(I_z - I_y) \\ \theta(I_z - I_x) \\ 0 \end{Bmatrix} \quad (4.28)$$

2. Aerodynamic Drag Torque

Aerodynamic drag is caused by the friction between the satellite as it orbits at an angular rate of ω_0 and the Earth's atmosphere. It is felt most below 500 km. The effects of drag cause a general decrease in angular velocity thereby resulting in decreasing altitude or orbital decay. The aerodynamic drag force is a function of air density, ρ ; velocity, V ; surface area perpendicular to the flight path, A ; and a dimensionless number called the coefficient of drag, C_D . [8]

$$F_D = \frac{1}{2} \rho V^2 C_D A \quad (4.29)$$

The orbital lifetime of a satellite is a function of altitude, h , and eccentricity, e . [7]

$$L = NP = 1.15185 \times 10^{-7} N \left(\frac{6378 + h}{1-e} \right)^{3/2} \quad (4.30)$$

where N is the estimated number of revolutions and P is the period of the orbit. The values of N can be obtained directly from Figure 4-6 where the ballistic coefficient for ORION is $m/(C_D A) = 132.87 \text{ kg/m}^2$. Note that the eccentricity for a circular orbit is zero, $e=0$. For ORION, orbital lifetime is shown in Figure 4-7 as a function of altitude. The linear velocity of a satellite equals

$$V = \omega_o R = (\mu/R)^{1/2} \quad (4.31)$$

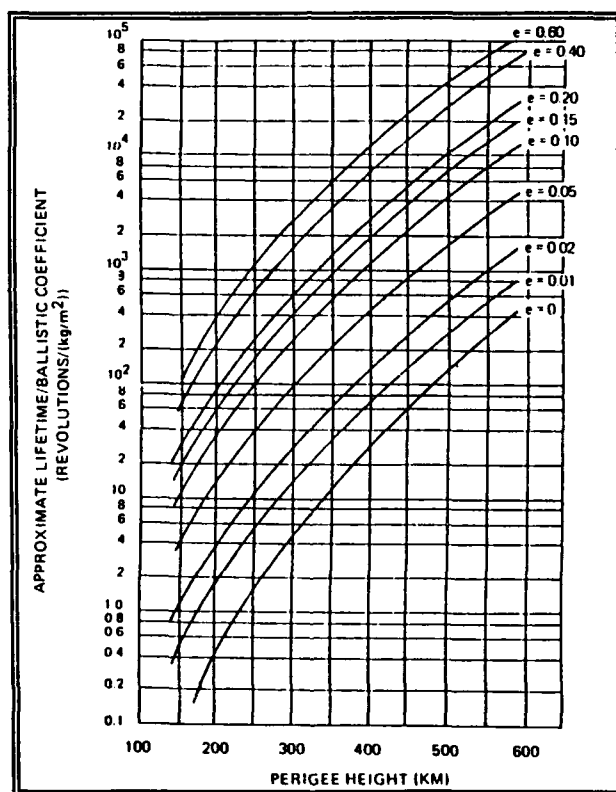


Figure 4-6 Orbital Decay [7]

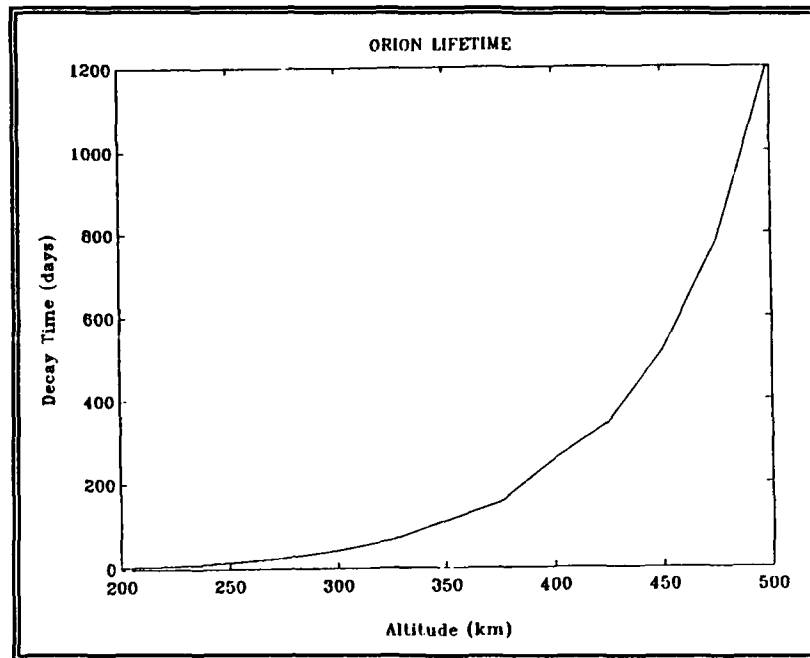


Figure 4-7 ORION Lifetime due to Aerodynamic Drag

where $R = R_e + h$, the altitude above Earth CM. The drag coefficient is between 1 and 2 in SI units. The value used for ORION will be $C_D=2$. The surface area of ORION perpendicular to the flight path is $A=.429\text{m}^2$. This reduces (4.29) to

$$F_D = 1.71 \times 10^{14} \rho / R \quad (4.32)$$

ORION drag torque will can be summed up as

$$T_{\text{drag}} = F_D L \cos\psi \quad (4.33)$$

where $L=.076m$ is the ORION center of pressure location along the y axis.[8] The effects of aerodynamic drag and gravitational gradient are simulated for a three-axis ORION in Chapter V.

C. SENSORS AND ACTUATORS

The ACS sensor suite is dictated by the type of stabilization, pointing accuracy, altitude, orbital parameters and cost constraints of the satellite budget. There are potentially three distinct stages of attitude control that ORION must handle. These include transfer orbit, acquisition and small error correction which includes altitude maintenance. If a transfer orbit is required, the satellite will most likely be spinning during this phase so different types of attitude determination sensors will be needed to accommodate spinning and non-spinning modes. In the acquisition stage, the satellite experiences large error rates which must be negated before accurate pointing can be sustained. The small error stage is the steady state operation that the satellite will undergo for the majority of its active life.

The attitude of a spacecraft in inertial space can be completely realized by two vectors as long as they are not colinear. Point sources such as the sun and stars afford excellent reference vectors while the Earth and planets present extended sources. Pitch, roll and yaw attitude errors

relative to the desired satellite orientation must be determined in addition to error rates about these three axes. Combinations of horizon and sun sensors can furnish position error while rate sensing gyros or error estimation routines can be used to resolve rate errors.

The current selection of attitude sensors for a spinning ORION consists of sun sensors, horizon sensors and magnetometers. The sun and horizon sensors provide the primary angular error output while the magnetometers act as back-up sensors. The spinning motion of the original satellite simplifies the number and cost of primary sensors by producing a periodic search motion. In a three-axis stabilized system this scanning motion must be integrated into the instrument in the case of the horizon sensor while multiple sun sensors with wider fields of view must be employed.

1. Horizon Sensors

Earth or horizon sensors are infrared devices that detect the 14-16 μm radiance profile of the earth as the space to earth and earth to space transitions occur. Horizon sensors can be used to ascertain pitch and roll errors. [2] Scanning or radiation balance detectors are employed in three-axis designs to provide a sweeping action across the disk of the Earth. Scanning sensors use two beams centered on a

reference line to scan the Northern and Southern hemispheres in an east-west direction. The scan pulse width is

$$pw = d / (2hw_h) \quad (4.34)$$

where d is the distance between horizon crossings, h is the satellite altitude and w_h is the scanning rate of the sensor. The difference between in-crossing to reference and reference to out-crossing pulse widths for each beam can be used to determine pitch error while the difference between Northern and Southern scans is proportional to roll error. An incremental pulse generator outputs a pulse at fractions of a degree for the known scan rate. Pulse width is computed by adding pulses from acquisition of signal (AOS) to reference then from reference to loss of signal (LOS). [7] Typical output from a scanning horizon sensor is depicted in Figure 4-8.

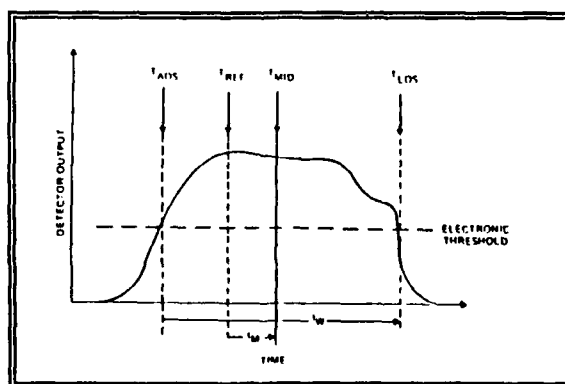


Figure 4-8 Output from a Scanning Horizon Sensor [7]

2. Sun Sensors

Since two non-coincidental directions are needed to measure alignment uniquely, it is necessary to find another reference vector besides that from the Earth. The sun or another star are logical alternatives since they can be approximated as point sources. Stars are the best inertial reference points and are not coplanar unless the inclination is zero and the orbital path is in the equatorial plane. Star sensors are orders of magnitude more complex, expensive and bulky than sun sensors which owe their simplicity to the close proximity of the most radiant body in the solar system.

Sun sensors are the most commonly used attitude sensor due to their relatively low cost, lightweight and broad application. [2] They can render accurate position error updates in harmony with horizon sensors when the satellite to Earth and satellite to sun vectors are non-parallel. Vector alignment can occur up to twice an orbit at local noon and midnight. Sun sensors are basically silicon solar cells with specialized masks for varying functions. Analog and digital sensors are available to measure the angle between the sun line and the pitch axis or sun presence in a particular field of view for instrument protection. The sun line vector is defined as

$$S = \sin\alpha\cos\delta I + \sin\delta J \cos\alpha\cos\delta K \quad (4.35)$$

where δ is the sun declination and α is the orbital angle of the satellite measured from local noon. Yaw errors about the pitch axis in the inertial frame can be expressed using

$$\mathbf{j} = -\psi\mathbf{I} + \mathbf{J} + \phi\mathbf{K} \quad (4.36)$$

for small angles. The sun angle, θ_s , is obtained by taking the dot product of the sun vector and \mathbf{j}

$$\cos\theta_s = \mathbf{S} \cdot \mathbf{j} = -\psi\sin\alpha\cos\delta + \sin\delta + \phi\cos\alpha\cos\delta \quad (4.37)$$

As the yaw error changes the sun angle varies

$$\frac{\partial \cos\theta_s}{\partial \psi} = -\sin\alpha\cos\delta \quad (4.38)$$

thus yaw error measurement is obtained. [2]

3. Magnetometers

Magnetometers are not a required sensor for current or future ORION designs. The original design utilizes booms with 2 lbm weights at the end to enhance the stability of the spinning satellite by altering the principal moments of inertia. Three of the tip weights are magnetometers which will provide a back-up attitude determination capability that dead weights cannot. Magnetometers are solenoid coils that

obey Faraday's Laws of Magnetic Induction. When placed in a time-varying magnetic field, solenoid coils will produce a voltage

$$V = \oint \mathbf{E} \cdot d\mathbf{l} = -AN\mu(dB_1/dt) \quad (4.39)$$

where E is the electromotive force, A is the cross-sectional area of the solenoid core, N is the magnetic permeability of the core and B_1 is the magnetic field component along the solenoid axis. The voltage is proportional to the magnetic field magnitude and direction. On-board control using magnetometers requires knowledge of the Earth's magnetic field at the orbit altitude. Knowledge of the magnetic field is not complete at low altitudes and too weak above 1000 km since the field strength decreases as the cube of the distance from the Earth's CM. [7]

4. Rate Gyroscopes

In the acquisition phase, some means of determining error rates is required before they can be cancelled. Rate sensing gyroscopes, Luenberger observers or Kalman filters for the sun and horizon sensor output are viable solutions. Rate integrating gyros (RIG) in triplets are the most accurate instruments used to detect error rates and positions about three axes. The output of a RIG is the current required to maintain the gyro gimbals at a null or zero position. The

current is proportional to the torque needed to zero the rates. The total angular momentum of a gyro is

$$H = LS + I_o \dot{\theta} O \quad (4.40)$$

where L is the magnitude of the angular momentum of the rotor about the spin axis and $I_o \dot{\theta}$ is the magnitude of the angular momentum of the gimbal system about the output axis. The nulling torque is

$$T_g = (dH/dt)_{gyro} + \omega \times H \quad (4.41)$$

Angular velocity in the gyro inertial frame is

$$\omega = \omega_I I + \omega_O O + \omega_S S \quad (4.42)$$

where I is the gyro input axis, S is the rotor spin axis and O is the output axis. Figure 4-9 depicts gyroscope operation and the physical location of the axes described by equations (4.40) and (4.42). The differential equation of motion for a gyroscope is

$$I_o \ddot{\theta} + D \dot{\theta} + K \theta - \omega_I L = 0 \quad (4.43)$$

where D is a viscous damping term and K is a restoring term.

[7]

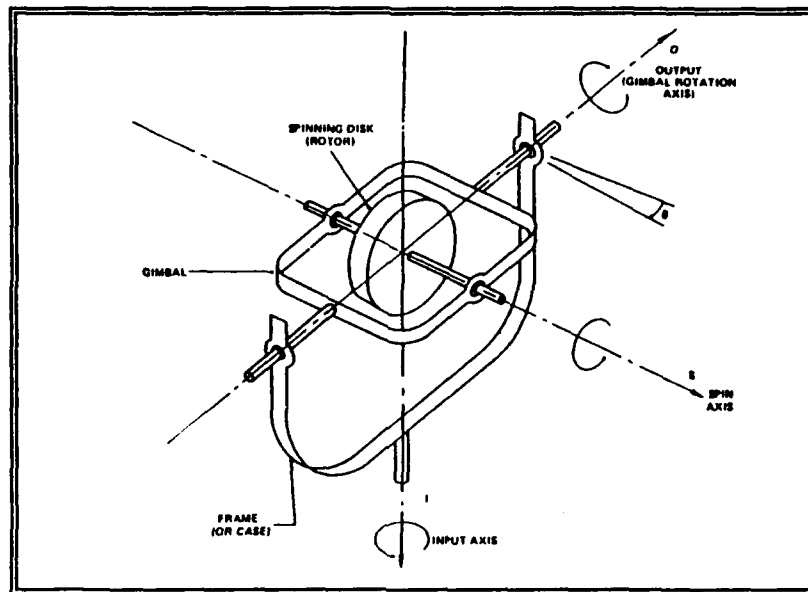


Figure 4-9 Single Degree of Freedom Gyroscope [7]

5. Hydrazine Thrusters

The functions of station keeping and attitude error correction are performed solely by control actuators called thrusters or reaction jets in this design. The thrusters on ORION use the monopropellant hydrazine with the Shell 405 catalyst for these functions. The hydrazine storage tank is pressurized with nitrogen. A basic hydrazine reaction jet is pictured in Figure 4-10.

The lifetime of a three-axis stabilized satellite is more acutely limited by the operational usefulness of the Shell 405 catalyst than in a spin stabilized vehicle where fuel usage can be more accurately predicted. The reaction jets on a three-axis stabilized satellite will be subjected to intermittent firing or low duty cycle firing. Thruster

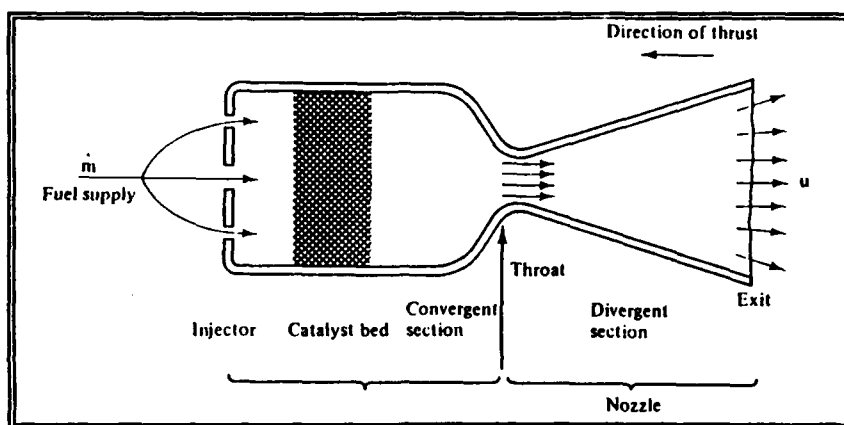


Figure 4-10 Basic Thruster Design [2]

performance is largely determined by the temperature of the catalyst bed. During steady state operation, intermittent firing of the jets will not allow the catalyst bed to maintain sufficient warmth to facilitate the most efficient thrust profile between firings. Typical values of specific impulse for hydrazine during transfer and steady state operation are 235 and 135 seconds, respectively. The specific impulse is seriously degraded in the steady state regime. Ultimately, this leads to the conclusion that the catalyst bed in a low duty cycle environment must be heated which requires considerably more power than just that used for opening and closing valves and heating the hydrazine to prevent freezing. [2]

In addition to the catalyst bed temperature, thruster performance is affected by impurities in the hydrazine that accumulate in the catalyst bed after each firing and variation in the nitrogen pressure as the propellant is depleted. [2]

Figure 4-11 shows the linear relationship between thrust obtainable and pressure.

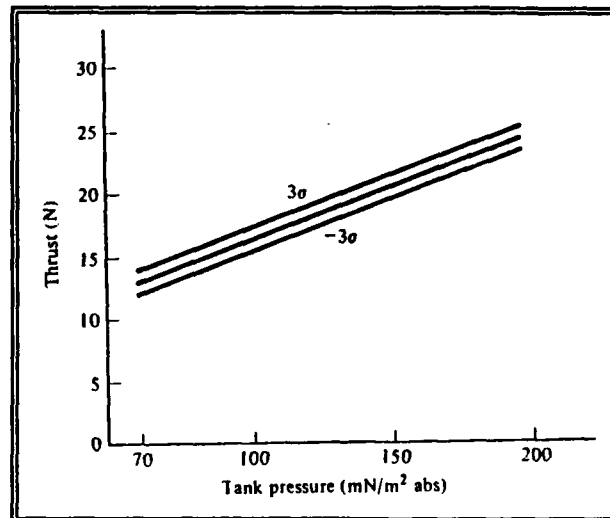


Figure 4-11 Thrust versus Tank Pressure [2]

A typical thruster profile is illustrated in figure 4-12. This profile assumes that physical conditions are acceptable, but that there is a finite delay between the time that the thruster is commanded on and the time that it reaches maximum thrust and likewise for the command off sequence. The time from t_1 to t_2 and t_4 to t_5 is a function of the valve opening and closing action. In Chapter V, the thruster profile is modeled as a pulse function for simplicity.

The current thruster selection for ORION includes a 40 lbf jet for orbital insertion and six .1 lbf attitude control jets. Figure 4-13 lists design specifications for these thrusters.

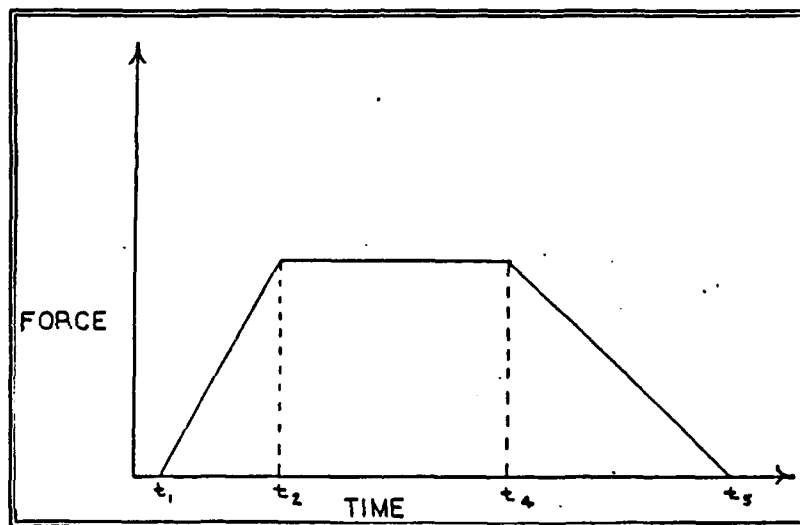


Figure 4-12 Typical Thrust Profile [8]

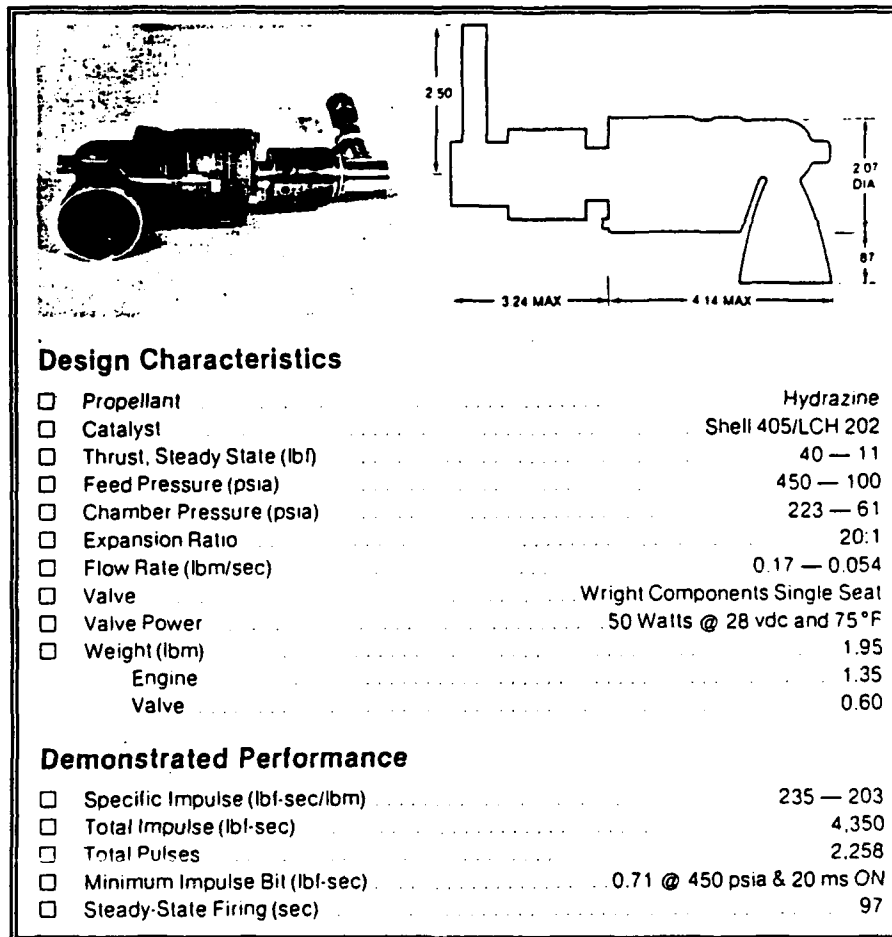


Figure 4-13a Rocket Research 40 lbf Thruster - Model 107B [1]

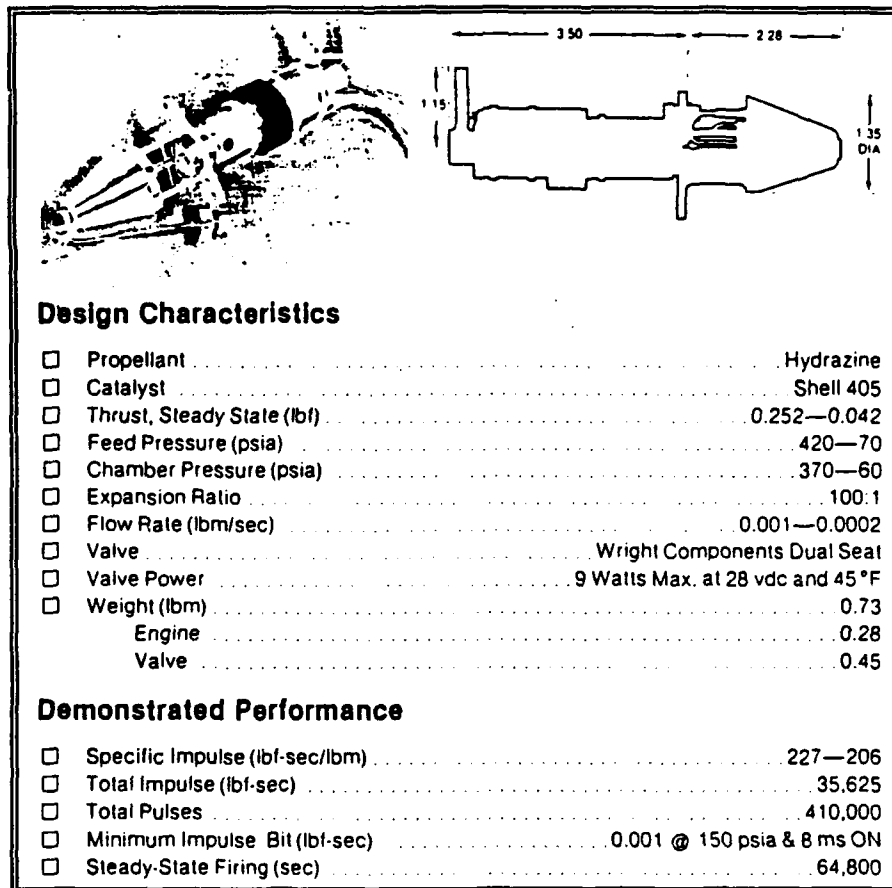


Figure 4-13b Rocket Research .1 lbf Thruster - Model 103C [1]

V. MINIMUM FUEL-TIME PROBLEM

Three-axis stabilization is inherently more expensive than spin stabilization due to the increase in complexity of attitude sensors and the energy necessary to maintain the desired pointing accuracy. For Orion this translates to more fuel needed once on-station than the original spinning version. This limits the total ΔV available for orbit transfer and the active on-station control life of the satellite. Therefore, the effective operational lifetime of the payload could be dictated by fuel constraints before other considerations. In order to conserve fuel and provide maximum operational lifespan, a minimum control effort solution using Pontryagin's minimum principle is explored in this section.

[9]

A. ON-STATION CONTROL LAW

For small angular rate and pointing errors, examination of one axis applies to all three axes. Thrusters are the sole control device for this design study and act independently in this case. The simplified differential equation for one axis is

$$I\dot{\omega} = T_c \quad (5.1)$$

where T_c is the thruster control torque and I is the inertia tensor with the products of inertia equal to zero. The normalized state equations for one axis are

$$\begin{bmatrix} \dot{x}_1(t) \\ \dot{x}_2(t) \end{bmatrix} = \begin{bmatrix} 0 & 1 \\ 0 & 0 \end{bmatrix} \begin{bmatrix} x_1(t) \\ x_2(t) \end{bmatrix} + \begin{bmatrix} 0 \\ 1 \end{bmatrix} u(t) \quad (5.2)$$

where x_1 is angular position, x_2 is angular velocity and u is the control torque provided by the thrusters. The minimum fuel performance index or cost function is

$$J(u) = \int_t (1 + \lambda |u|) dt \quad (5.3)$$

where λ is a weighting factor applied to the control. As $\lambda \rightarrow 0$, the performance index becomes the minimum time solution and as $\lambda \rightarrow \infty$, the performance index approaches the pure minimum fuel solution. Since any minimum effort problem is a trade off between elapsed time and consumed fuel both should be considered and are represented by (5.3). The performance measure must be minimized to obtain the optimal solution for given initial conditions and final states, $x(t_f)=0$. Every value of the weighting factor provides a minimal trajectory. The selection of the weighting factor is determined by reasonable transient time and fuel expenditure. The normalized admissible controls for thruster operation are

$$|u(t)| < T_c/I = N \quad (5.4)$$

where T_c is the maximum torque available from the reaction jets. The cost function for thruster operation is called 'Bang-Off-Bang' since the satellite drifts before a final control torque is applied to bring it to the desired final attitude. The Hamiltonian for (5.3) is defined as

$$H(x,u,p,t) = 1 + \lambda |u| + p_1 x_2 + p_2 u \quad (5.5)$$

where $p(t)$ are Lagrange multipliers. The costate equations are

$$\begin{aligned} \dot{p}_1(t) &= -\partial H/\partial x_1 = 0 \\ \dot{p}_2(t) &= -\partial H/\partial x_2 = -p_1(t) \end{aligned} \quad (5.6)$$

which have solutions

$$\begin{aligned} p_1(t) &= c_1 \\ p_2(t) &= -c_1 t + c_2 \end{aligned} \quad (5.7)$$

The Hamiltonian must be minimized on an optimal trajectory, so the form of optimal control is

$$u(t) = \begin{cases} N & p_2 < -\lambda \\ 0 & -\lambda \leq p_2 \leq \lambda \\ -N & p_2 > \lambda \end{cases} \quad (5.8)$$

where switching occurs at $|p_2|=\lambda$. The effect that any known or unknown torque has on the satellite can be best illustrated in the phase plane. This is a plot of angular position versus velocity as a function of applied torque. There are essentially two switching curves for the given minimum trajectory. These correspond to a curve that is dependent on the weighting factor, λ , and the minimum time curve as shown in the phase plane representation in Figure 5-1.

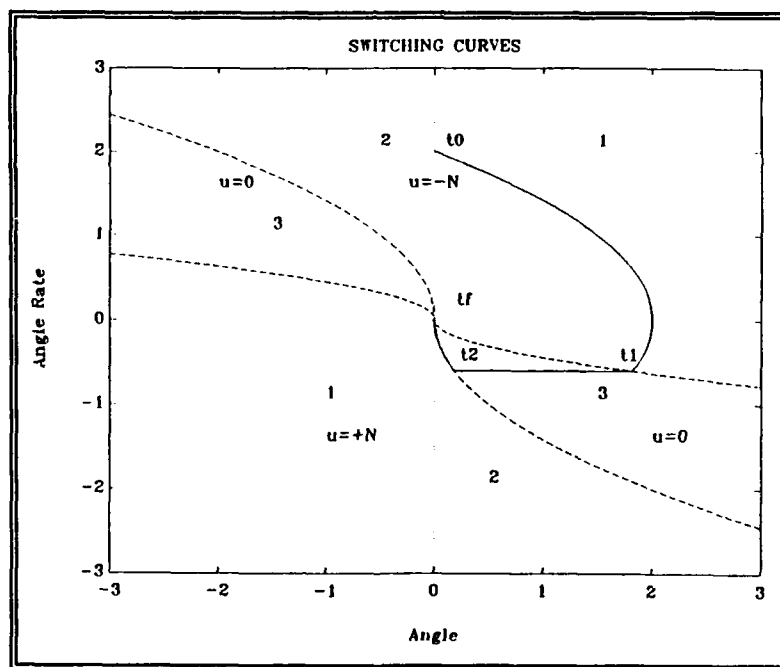


Figure 5-1 Double Switching Curve Control Law

If the initial conditions place the satellite in region 1, a negative torque is applied until t_1 , when region 3 is entered

and control is turned off. Positive control is applied at t_2 , when the satellite reaches region 2, which is the switching curve for the minimum time solution. The reverse is true if the initial conditions place the satellite in region 2. At t_1 the control goes off, $u(t_1)=0$, and (5.6) becomes

$$p_2(t_1) = \lambda = -c_1 t_1 + c_2 \quad (5.9)$$

The position continues to change as a function of velocity at turn-off. After t_2 , control is turned on, $u(t_2)=0$, and the satellite ideally moves to the desired position. At t_2 (5.9) becomes

$$p_2(t_2) = -\lambda = -c_1 t_2 + c_2 \quad (5.10)$$

Subtracting (5.10) from (5.9)

$$(t_2 - t_1) = 2\lambda/c_1 \quad (5.11)$$

Assuming that velocity is constant at turn-off, $\dot{x}_2=0$

$$x_2(t_1) = x_2(t_2) = x_2(t)$$

Solving the Hamiltonian at the switching times and substituting (5.6) for p_1 yields

$$H(t_1) = H(t_2) = 0$$

$$H(t_1) = 1 - c_1 x_2(t_1) = 0$$

$$c_1 = \frac{1}{x_2(t_1)} \quad (5.12)$$

Substituting (5.11) into (5.12)

$$(t_2 - t_1) = 2\lambda x_2(t_1) \quad (5.13)$$

Solving the state equation, $\dot{x}_1(t) = x_2(t)$

$$x_1(t_2) - x_1(t_1) = x_2(t_1) [t_2 - t_1] \quad (5.14)$$

From t_2 to t_f the satellite follows a minimum time trajectory where

$$x_1(t) = -\frac{1}{2} \frac{x_2^2(t)}{|N|} \quad (5.15)$$

Substituting (5.13) and (5.15) into (5.14)

$$x_1(t) + \frac{(4\lambda + 1)}{2|N|} x_2^2(t) = 0 \quad (5.16)$$

which is the control law for this minimum fuel problem.

Equation (5.16) becomes usable in all quadrants when $x_2^2 = x_2|x_2|$ which takes the sign of x_2 into account. Figure 5-2 demonstrates minimum trajectories for various values of λ . The initial conditions $x_1(0)=1, x_2(0)=0$ were used to test for minimization of the selected cost function. As shown in figure 5-3, the minimum value of the chosen cost function occurs at $\lambda=2.25$ when this value is substituted into equation (5.16).

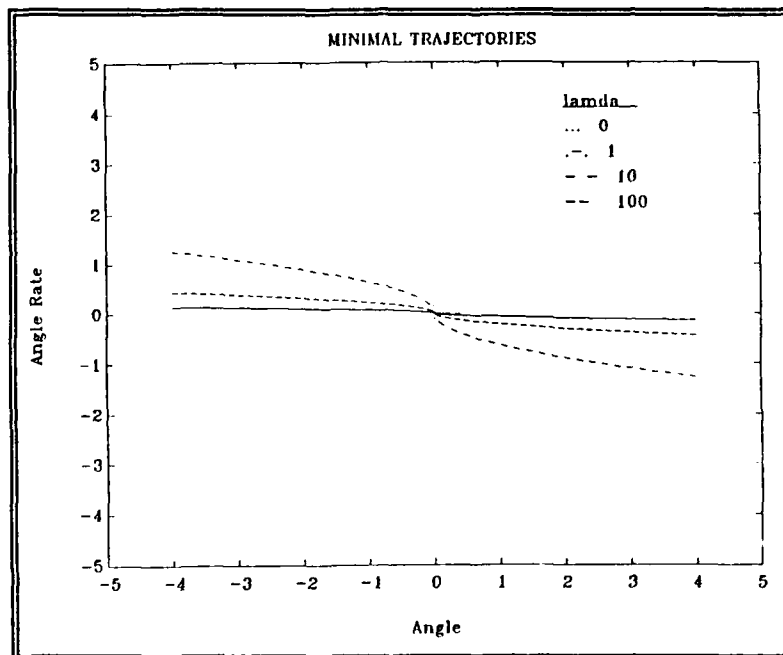


Figure 5-2 Parabolic Switching Curves for $\lambda=0,1,10,100$

Figure 5-4a is a time response of angular position and rate. Figure 5-4b is the time response of control torque. Notice that thruster chatter occurs at the end of the cycle, since fine control near the desired attitude is not implemented.

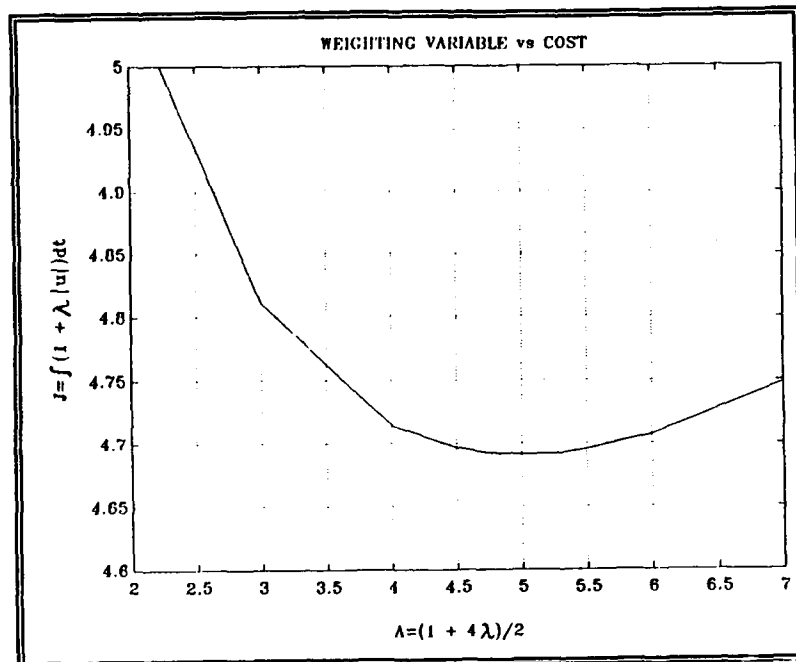


Figure 5-3 Minimum Fuel-Time Cost Function
 $J = \int (1 + 2.25|u|) dt$

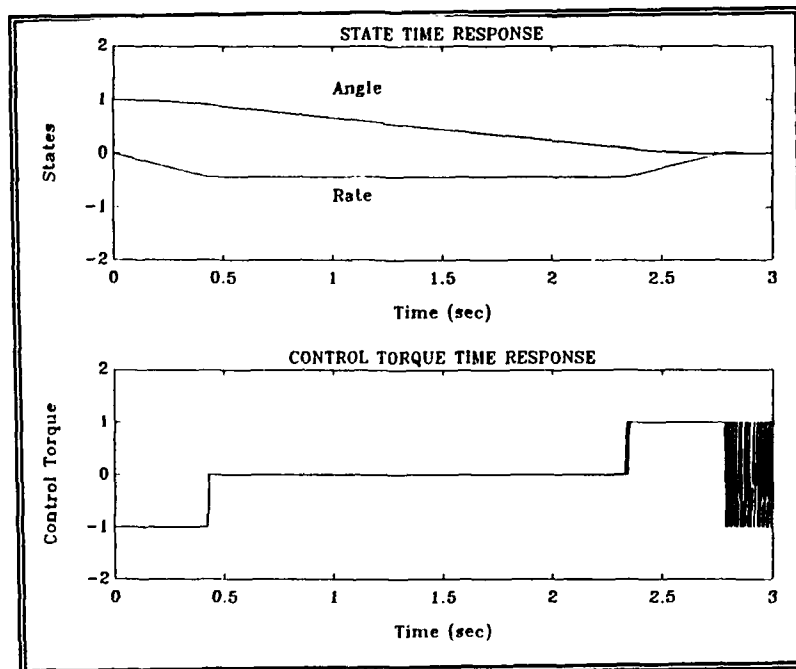


Figure 5-4 Time Response of States and Control

Figure 5-4b shows the "bang-deadzone-bang" behavior of the control law. Figure 5-5 is a phase plane representation of the same cycle.

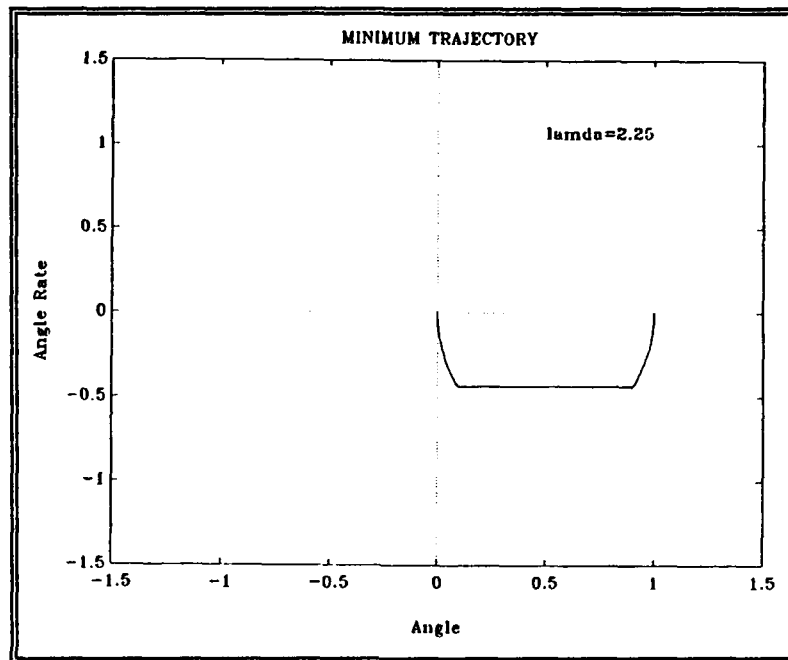


Figure 5-5 Phase Plane for $\lambda=2.25$

B. LIMIT CYCLE CONTROL

Ideally, the last thrust period will take the satellite to the origin, but this is a function of the integration step size. A similar analogy exists for the thruster in the form of the minimum impulse bit available. Physically angular rates are never zeroed, but they can be maintained in a region. Satellite motion is then dictated by a finite limit cycle even in the absence of external disturbances.

While in the limit cycle attitude errors are reduced below specified values. The fine tuning region is determined by

pointing accuracy requirements, but it is also a function of minimum jet impulse for angular velocity and the precision or noise contribution of the attitude sensor instrumentation. Minimum jet impulse is a measure of the smallest thrust unit available when the control valves are immediately opened and closed, i.e., the shortest single jet pulse. In order to increase the coasting period in the limit deadzone, the satellite rate must be reduced to the lowest value possible without causing thruster chatter. Chatter is a constant cycling of opposing thrusters when limits are exceeded after each firing. The limit cycle for the cost function simulated in this example is depicted in Figure 5-6.

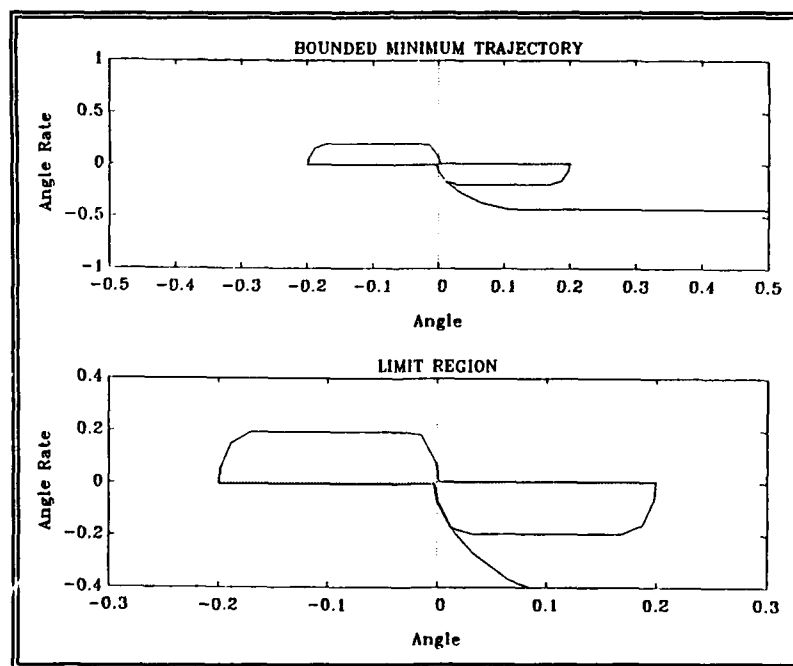


Figure 5-6 Limit Cycle

A third switching curve was implemented in the boundary region only to minimize fuel expended while cycling. The third switching curve has a flatter slope, $\lambda=250$, and thus a wider deadzone. The best deadzone obtainable is again limited by the minimum jet impulse available from the thrusters. Figure 5-7 utilizes the third switching curve and can be compared to Figure 5-6 where only two switching curves were realized to demonstrate the improved fuel consumption.

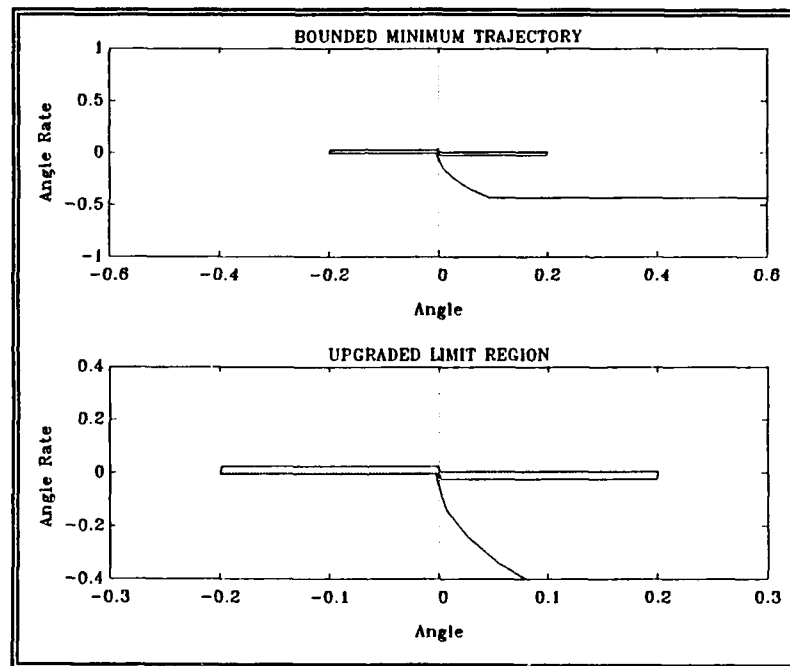


Figure 5-7 Upgraded Limit Cycle

Figure 5-8 shows the time responses of thruster operation during fine tuning in both cases. Note the single impulse firing that occurs at the edge of the limit boundaries when the third switching curve is implemented. The appendix

provides a description of the Tutsim program that simulates the independent control law about a single axis.

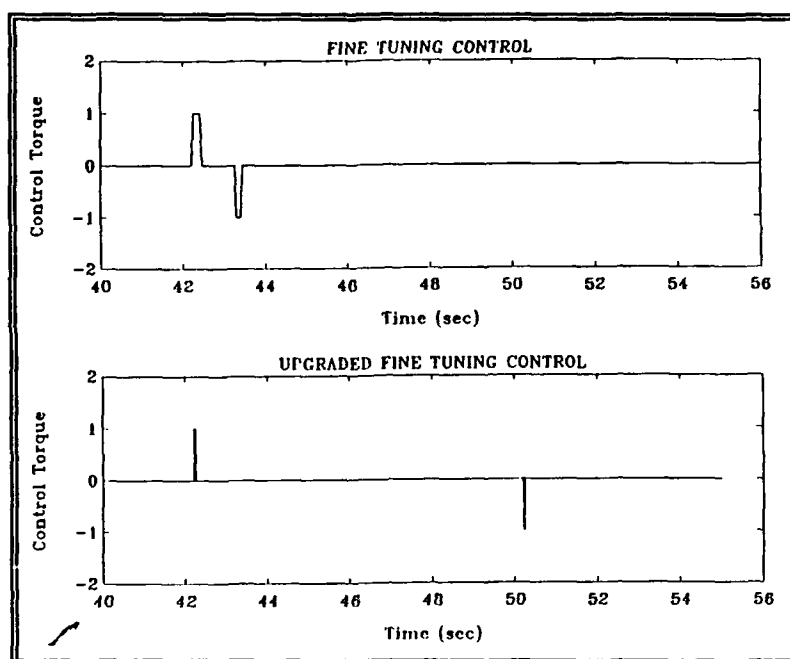


Figure 5-8 Fine Control

C. ACQUISITION PHASE CONTROL

The acquisition phase is the most critical aspect of satellite operation after a successful launch. During acquisition, the satellite may be tumbling. Tumbling translates to high error rates which will cause coupling about at least two axes. In this phase, a minimum time solution is desired to cancel the excess rates quickly. [6] The Euler moment equations of motion are

$$\begin{aligned}
\dot{I}_x \omega_x &= (I_y - I_z) \omega_y \omega_z + T_x \\
\dot{I}_y \omega_y &= (I_z - I_x) \omega_x \omega_z + T_y \\
\dot{I}_z \omega_z &= (I_x - I_y) \omega_x \omega_y + T_z
\end{aligned}
\tag{5.17}$$

where T_x , T_y and T_z are the control torques; the product of thrust and moment arm. If a single axis of symmetry is assumed, as is the case for a cylinder, two of the moments of inertia will be equal

$$I_x = I_z = I$$

The moment equations become

$$\begin{aligned}
\dot{\omega}_x &= \alpha \omega_y \omega_z + u_x \\
\dot{\omega}_y &= u_y \\
\dot{\omega}_z &= -\alpha \omega_y \omega_x + u_z
\end{aligned}
\tag{5.18}$$

where $\alpha = (I - I_y)/I$ and $u_i = T_i/I_i$.

Motion about the axis of symmetry is independent of the other two axes and is controlled at all times as discussed in the previous section. Assuming that ω_y is constant when u_y is zero during rate reduction, the state equations become

$$\begin{bmatrix} \dot{x}_1(t) \\ \dot{x}_2(t) \end{bmatrix} = \begin{bmatrix} 0 & \beta \\ -\beta & 0 \end{bmatrix} \begin{bmatrix} x_1(t) \\ x_2(t) \end{bmatrix} + \begin{bmatrix} 1 & 0 \\ 0 & 1 \end{bmatrix} u(t)
\tag{5.19}$$

where $\beta = \alpha \omega_y$, $x_1 = \omega_x$, $x_2 = \omega_z$, $u_1 = u_x$ and $u_2 = u_z$. The minimum time cost function is

$$J = \int_t dt \quad (5.20)$$

The Hamiltonian for the coupled system using both controllers, u_1 and u_2 , is

$$H(x, u, p, t) = 1 + p_1 x_2 - p_2 x_1 + p_1 u_1 + p_2 u_2 \quad (5.21)$$

for $\beta=1$. The costate equations are

$$\begin{aligned} \dot{p}_1(t) &= -\partial H / \partial x_1 = p_2(t) \\ \dot{p}_2(t) &= -\partial H / \partial x_2 = -p_1(t) \end{aligned} \quad (5.22)$$

which have solutions

$$\begin{aligned} p_1(t) &= c_3 \cos(t+\delta) \\ p_2(t) &= c_4 \sin(t+\delta) \end{aligned} \quad (5.23)$$

To minimize the Hamiltonian on an optimal trajectory, the form of optimal control is

$$\begin{aligned} u_1(t) &= -\text{sign}(p_1) \\ u_2(t) &= -\text{sign}(p_2) \end{aligned} \quad (5.24)$$

The control torque of each set of thrusters will reverse every half cycle while the control mix will change every quarter cycle. The minimum time switching curves can be derived using

$$\frac{dx_1}{dx_2} = \frac{x_2 + u_1}{-x_1 + u_2} \quad (5.25)$$

$$\int (-x_1 + u_2) dx_1 = \int (x_2 + u_1) dx_2$$

$$\frac{x_1^2}{2} - u_2 x_1 = \frac{-x_2^2}{2} - u_1 x_2$$

Adding $u_2^2 + u_1^2$ to both sides of (5.25) and multiplying by two, yields

$$(x_1 - u_2)^2 + (x_2 + u_1)^2 = u_1^2 + u_2^2 \quad (5.26)$$

For normalized control torque, $u_1 = \pm 1$, $u_2 = \pm 1$, (5.26) becomes

$$(x_1 \mp 1)^2 + (x_2 \pm 1)^2 = 2 \quad (5.27)$$

Equation (5.26) describes four circles with their centers at $(\pm 1, \pm 1)$ in each quadrant. The switching curves are defined as the quarter of each circle that intersects the abscissa and ordinate in each quadrant as shown in Figure 5-9. Beyond these scalloped sections the switching curves are mirror

images of the half sinusoidal sections along each axis, but minimal error is experienced if switching is implemented about the axes themselves.

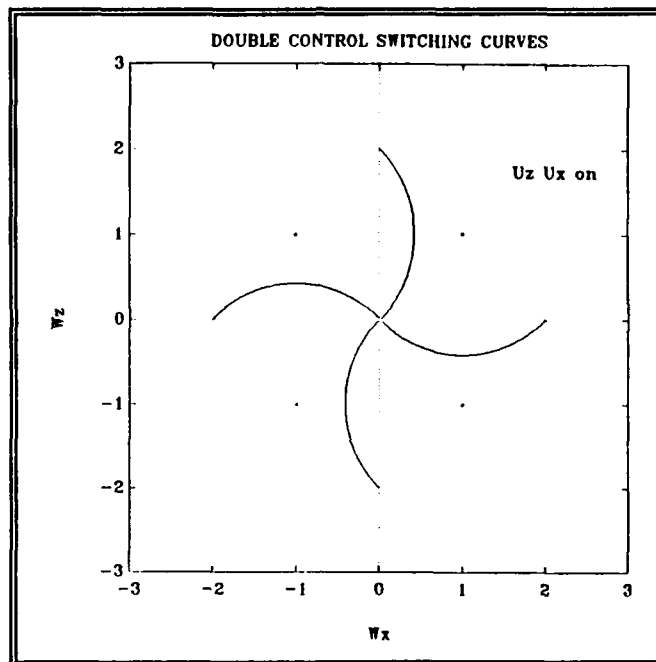


Figure 5-9 Double Controller Minimum Time Switching Curves

A phase plane representation is used to illustrate rate reduction where ω_x is the abscissa and ω_z is the ordinate. Figure 5-10 depicts the implementation of the four quarter section switching curves in a circular region with a radius of two for initial rate conditions of $(\pm 1.5, \pm 1.5)$. Figure 5-11 portrays switching about the coordinate axes in the region beyond a radius two. In the outer region, $u_x = -\text{sign}(\omega_x)$ and $u_z = -\text{sign}(\omega_z)$. Figure 5-12 shows the control torque time response for u_x and u_z .

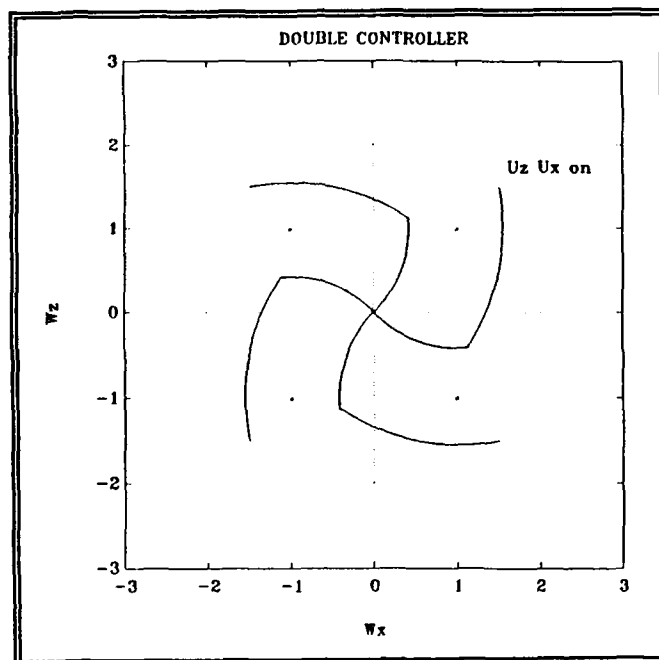


Figure 5-10 Inner Region Switching

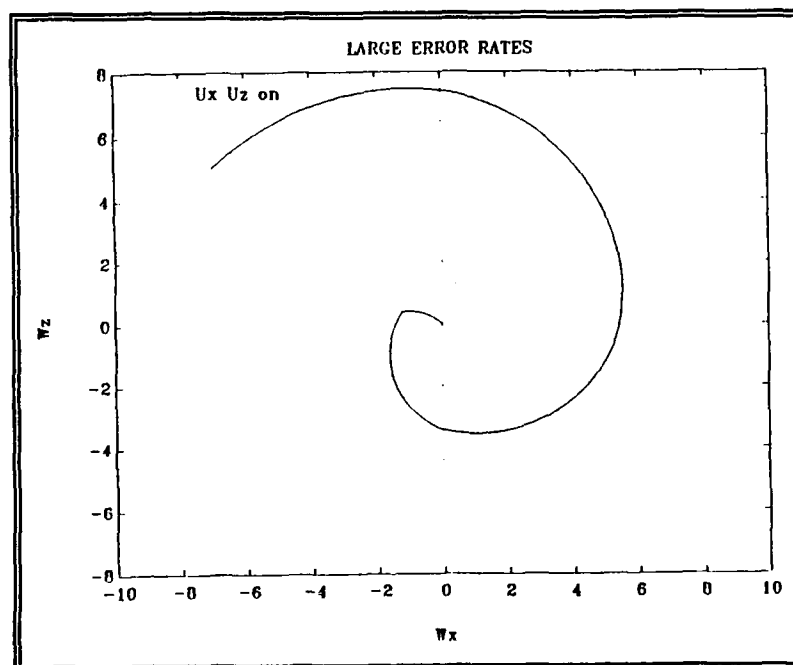


Figure 5-11 Outer Region Switching
a) $\omega_x = \omega_z = 6$ b) $\omega_x = -7$ $\omega_z = 5$

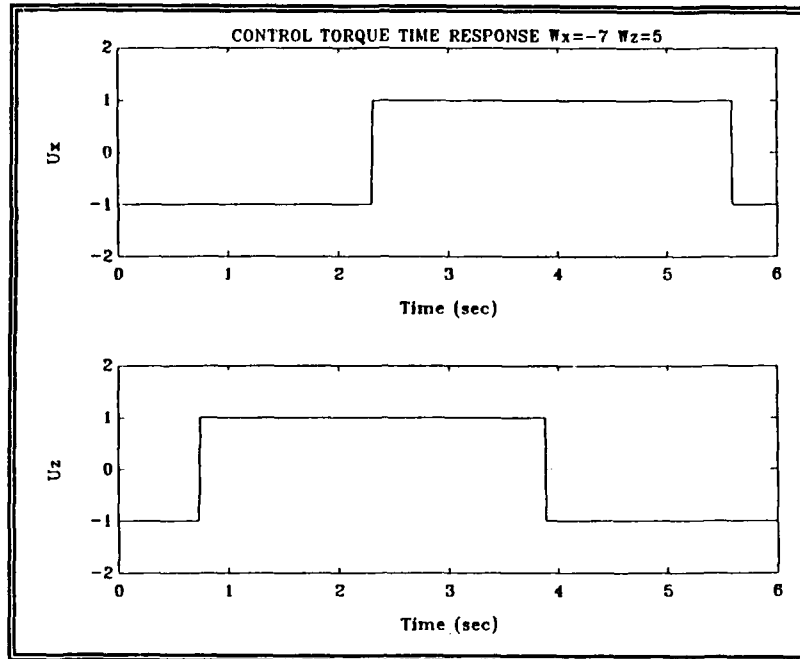


Figure 5-12 Outer Region Control

Since the system is coupled, only one controller is needed to reduce the rates about both axes. If $u_1 = 0$, equation (5.25) becomes

$$\frac{x_1^2}{2} - u_2 x_1 = \frac{-x_2^2}{2} \quad (5.28)$$

Adding u_2^2 to both sides and multiplying by two

$$(x_1 - u_2)^2 + x_2^2 = u_2^2 \quad (5.29)$$

which becomes

$$(x_1 \mp 1)^2 + x_2^2 = 1 \quad (5.30)$$

for $u_2=\pm 1$. Conversely, for $u_2=0$ equation (5.30) becomes

$$x_1^2 + (x_2^2 \pm 1) = 1 \quad (5.31)$$

for $u_1=\pm 1$. Equations (5.30) and (5.31) describe two symmetric circles with centers at $x_1=\pm 1$ and $x_2=\pm 1$, respectively. The switching curves for the minimum time solution are the half circles shown in Figure 5-13. Figure 5-14 demonstrates rate reduction for a single controller system. For initial rates in the outer region, switching about the axes was implemented. Control torque values of $u_2=\text{sign}(\omega_x)$ for (5.30) and $u_x=\text{sign}(\omega_z)$ for (5.31) were applied. Figure 5.15 demonstrates large rate error reduction for both single controller cases.

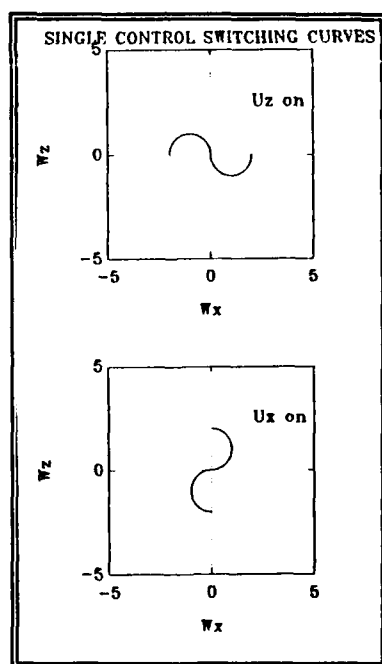


Figure 5-13 Single Controller Switching Curves

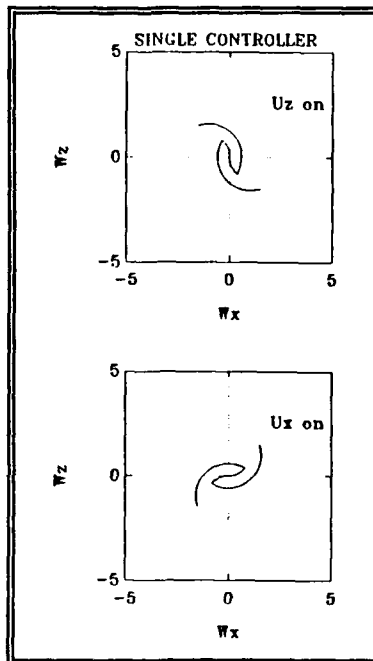


Figure 5-14 Single Control for $\omega_x = \omega_z = \pm 1.5$

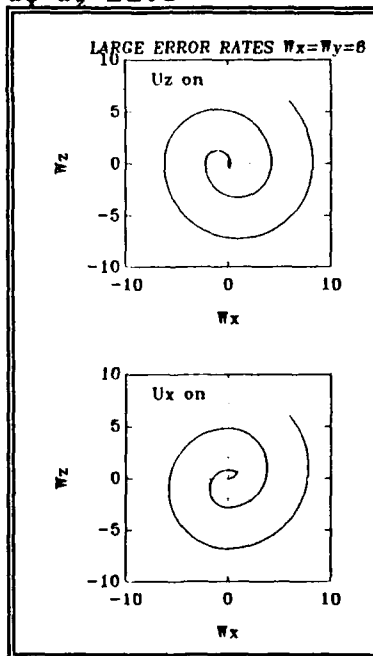


Figure 5-15 Outer Region $\omega_x = \omega_z = 6$

Figure 5-16 illustrates the control torque time responses in the outer region. Comparison of Figures 5-12 with 5-16 shows that the double controller system takes half the time using the same amount of control effort as the single controller system.

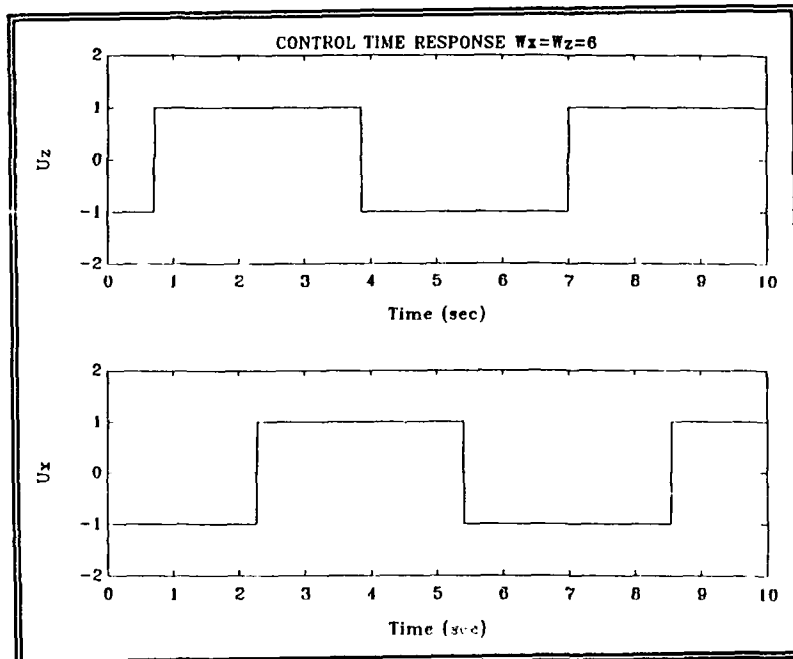


Figure 5-16 Outer Region Control Torque

D. LIMIT CYCLE CONTROL FOR ORION

ORION specifications can easily be implemented in the simulation described in previous sections. A three-axis stabilized ORION will be oriented such that the yaw axis is colinear with the longitudinal axis. The symmetry of the principal moments of inertia becomes $I_x=I_y$, vice $I_x=I_z$, as in the spin stabilized configuration. ORION principal moments of inertia from Table 4-1 are

$$I_x \approx I_y \approx 6.753 \text{ kg-m}^2$$

$$I_z = 2.776 \text{ kg-m}^2$$

Attitude control thruster data is obtained from Figure 4-14b. The thrust available from the attitude control reaction jets is between .24 and 1.068 Newtons. The minimum impulse bit is .0223 N-sec for .025 seconds. The total pulses available as a function of the catalyst effective lifetime are 161,000. The mass flow rate of the thrusters is between .104 and .453 grams/sec.

Torque is the product of thrust and moment arm. The length and radius of the ORION cylinder are .889 and .2414 meters, respectively. Thrusters operate in pairs to prevent translational movement so the average torque produced for ORION is

$$T_x = T_y = 2(.445)(.889) = .7912 \text{ N-m}$$

$$T_z = 2(.445)(.2414) = .2148 \text{ N-m}$$

The control accelerations are

$$u_x = u_y = .1172 \text{ s}^{-2}$$

$$u_z = .0774 \text{ s}^{-2}$$

Pointing accuracies of $\pm 1^\circ$ and $\pm 0.05^\circ/\text{sec}$ were used in the example illustrated to define the limit region. The minimum fuel-time switching curves were implemented with the values of λ previously used, $\lambda=2.25$ and 250 for the outer region deadzone and limit region deadzone switching curves, respectively. Figures 5-17 and 5-18 illustrate the minimum fuel-time control law for yaw and roll-pitch when ORION values for torque and moments of inertia are used.

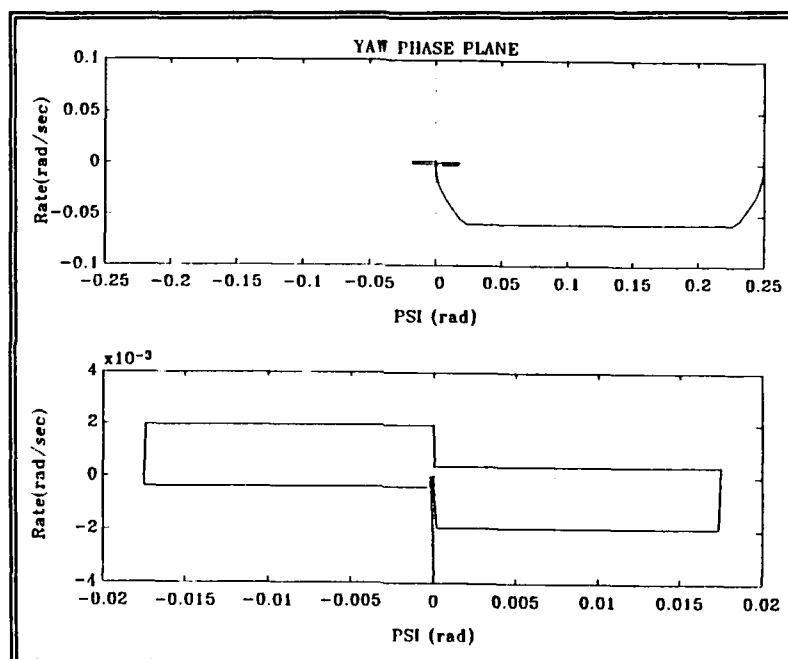


Figure 5-17 Yaw Limit Cycle for Limits of $\pm 1^\circ$, $\pm 0.05^\circ/\text{sec}$

Figure 5-19 shows the yaw thruster operation for initial conditions of angle = .25 rad and zero rate.

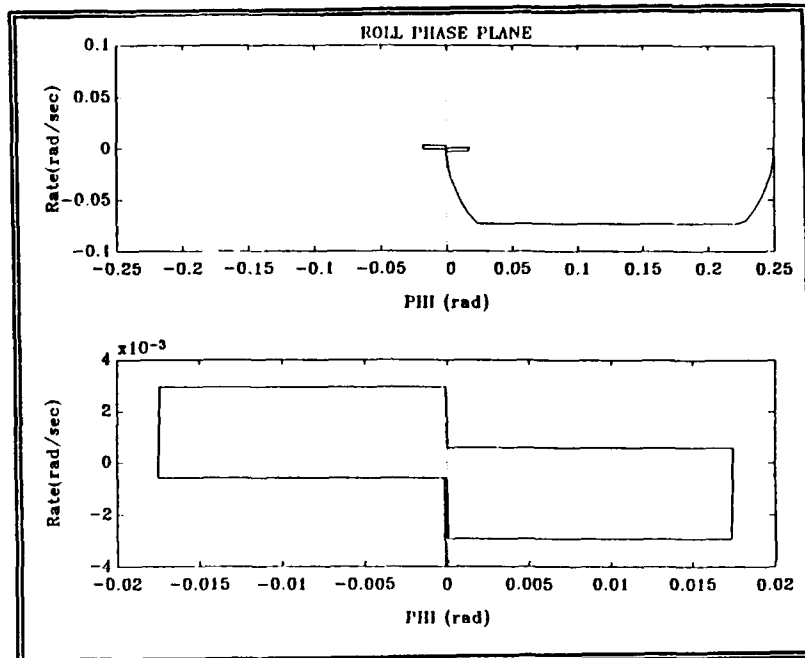


Figure 5-18 Roll-Pitch Limit Cycle for Limits of $\pm 1^\circ$, $\pm .05^\circ/\text{sec}$

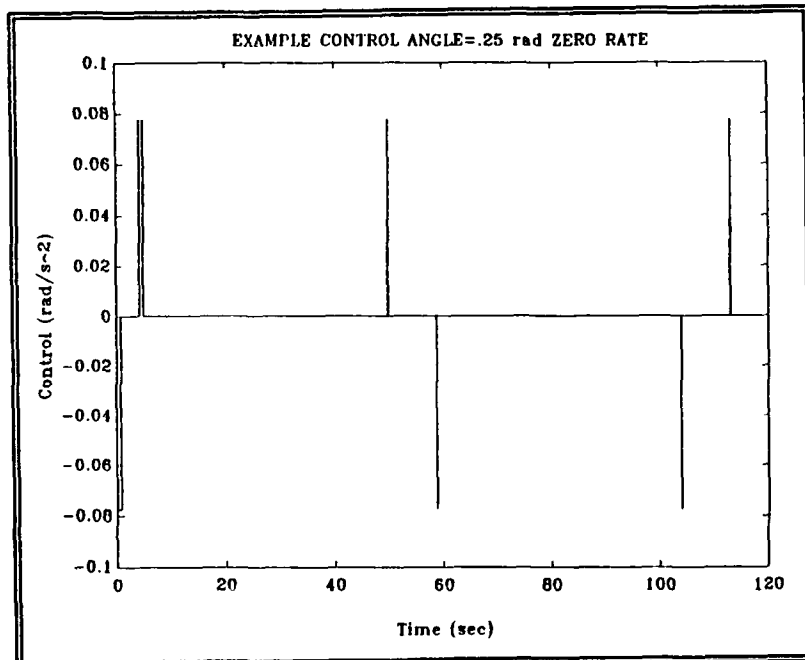


Figure 5-19 Yaw Thruster Operation angle=.25, zero rate

It is difficult to predict fuel usage up to the operational phase of flight for three-axis control. The approximate limit cycle lifetime with all thrusters operating is

$$L = \frac{\text{Total Fuel Available}}{\text{Fuel per Control Cycle}} \Delta t \quad (5.32)$$

where Δt = one limit cycle. [1] In the limit cycle, with no environmental disturbances added, individual pairs of thrusters pulse on four times per cycle. Using a mass flow rate of .104 grams/s for .025 sec, the minimum pulse time, gives a total fuel per control cycle of between .0624 and .0832 grams if all six thrusters are operating to maintain attitude in their respective limit regions. The yaw and roll-pitch control cycle duration for this example are 108 and 72 seconds, respectively. Assuming that 2/3 of the original 32.35 kg of hydrazine is available for limit cycle attitude control, total limit cycle lifetime would be about 320 days. Approximate limit cycle lifetimes for various combinations of weighting factors, rate limits and minimum impulse bits based on the hydrazine budget are listed in Table 5-1. Increasing the value of λ or decreasing the rate error limit will decrease the rate error and thus lengthen the thruster off time, but the maximum effective value of λ is limited by the the minimum impulse bit on-period. For the thruster used

Table 5-1 LIMIT CYCLE LIFETIMES

u_z	$\Delta t_z(\text{sec})$	rate($^\circ/\text{sec}$)	λ	$\Delta t_{cz}(\text{sec})$	L(days)
.0774	.025	.075	100	48	143
.0774	.01	.05	250	108	323
.0774	.01	.025	1000	125	427
.0774	.006	.015	1000	185	632
.0387	.025	.075	100	86	257
.0387	.025	.075	1000	94	281
.0387	.01	.015	1000	218	869

u_{xy}	$\Delta t_{xy}(\text{sec})$	rate($^\circ/\text{sec}$)	λ	$\Delta t_{cxy}(\text{sec})$
.1172	.025	.085	100	30
.1172	.025	.05	250	72
.1172	.007	.025	1000	112
.1172	.004	.015	1000	180
.0586	.025	.075	100	58
.0586	.025	.075	1000	64
.0586	.008	.015	1000	195

in this example, $\lambda > 100$ has negligible effect since the minimum ΔV imparted is

$$\Delta V_z = u_z \Delta t = .0774(.025) = .001935 \text{ rad/sec}$$

$$\Delta V_{xy} = u_{xy} \Delta t = .1172(.025) = .00293 \text{ rad/sec}$$

which will kick the rate error from the negative limit of -8.73×10^{-4} rad/sec to a positive value of .0012 rad/sec. The example illustrated in the figures uses an integration step size of .01 seconds. In order to implement the fuel saving choices listed in table 5-1 attitude control thrusters with smaller minimum impulse bits and/or on-times must be utilized.

Limit cycle lifetime based on the number of available pulses ranges from 30 to 90 days. This is considerably less than limit cycle lifetimes based on fuel consumption. In addition to smaller impulse bits, the number of available pulses must increase to lengthen the active life of ORION. Another option would be to operate for specified periods during each orbit vice continuously. Rather than replacing the thrusters with more complex and expensive items, this could increase the active lifetime of the existing design to acceptable levels.

E. ENVIRONMENTAL DISTURBANCE EFFECTS

Since the majority of the satellite lifetime will be spent in the operational or steady state mode, this is the phase when the effects of the external disturbances of gravity gradient and aerodynamic drag will play the largest part. Substituting the small angle approximation for the angular velocity vector and adding a disturbance moment to the Euler Moment Equations yields

$$\begin{aligned}\ddot{\phi} &= \alpha \omega_o^2 \phi + u_x + D_x \\ \ddot{\theta} &= u_y + D_y \\ \ddot{\psi} &= u_z + D_z\end{aligned}\tag{5.33}$$

where $\alpha = (I_y - I_z)/I_x$, $D_1 = T_{D1}/I_1$ is the disturbance contribution and $u_1 = T_{C1}/I_1$ is the control offering. The small angle approximations for the gravity gradient moment equations are

$$T_G = 3\omega_o^2 \begin{Bmatrix} \phi (I_z - I_y) \\ \theta (I_z - I_x) \\ 0 \end{Bmatrix} \quad (5.34)$$

where the orbital rate $\omega_o^2 = \mu_e/R^3$. Figure 5-20 shows the orbital rate versus altitude for any satellite orbiting the Earth.

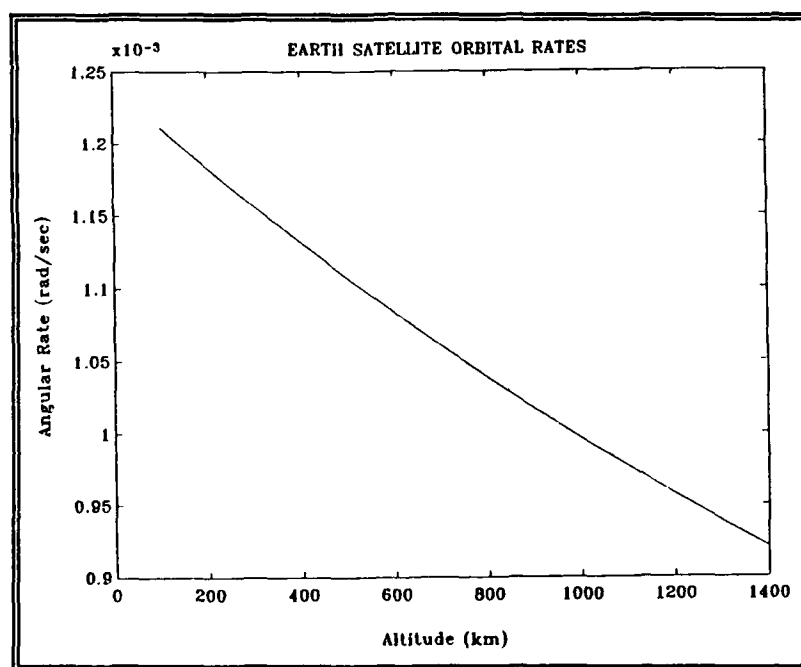


Figure 5-20 Orbital Rate, ω_o , versus altitude

Substituting (5.34) into (5.33) and eliminating the control term gives

$$\ddot{\phi} = -2\omega_o^2 \left(\frac{I_y - I_z}{I_x} \right) \phi \quad (5.35)$$

$$\ddot{\theta} = 3\omega_o^2 \left(\frac{I_z - I_x}{I_y} \right) \theta$$

which are equations of motion for simple harmonic oscillators. The moment of inertia ratios for ORION equal +.5929 and -.5929, respectively. Figures 5-21 and 5-22 illustrate the harmonic motion about the roll and pitch axes. Plots in 5-21a and 5-22a are phase plane representations while graphics in 5-21b and 5-22b show the time response for angle and rate. The motion is stable and periodic with a period that corresponds to the satellite orbit. The orbital period is defined as [4]

$$P = \frac{2\pi}{(\mu)^{1/2}} R^{3/2} \quad (5.36)$$

Figure 5-23 furnishes the orbital period versus altitude for an Earth orbiting satellite. In Figures 5-21 and 5-22 the maximum rate error induced never exceeds the initial value, but the angle error will exceed the desired pointing accuracy over the course of an orbit if a rate error exists. Gravity gradient torque has a time constant that is equivalent to an orbital period. The time constant of this all-thruster

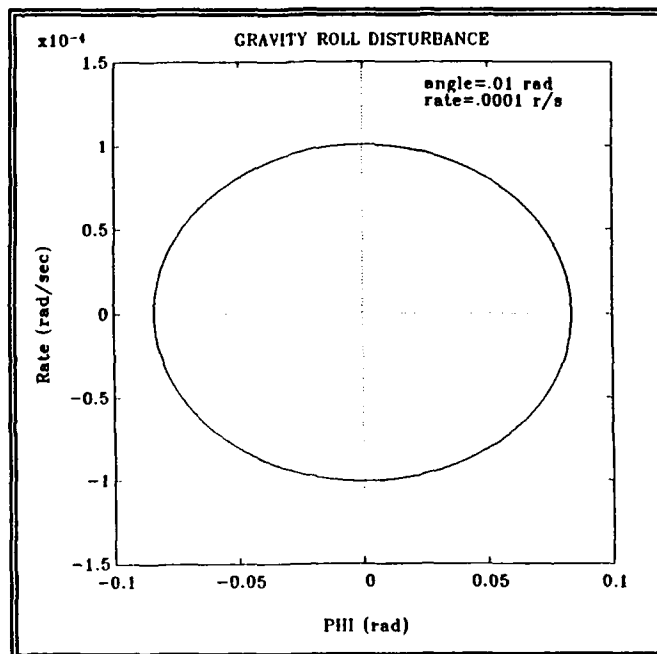


Figure 5-21a Gravitational Roll Effects Phase Plane

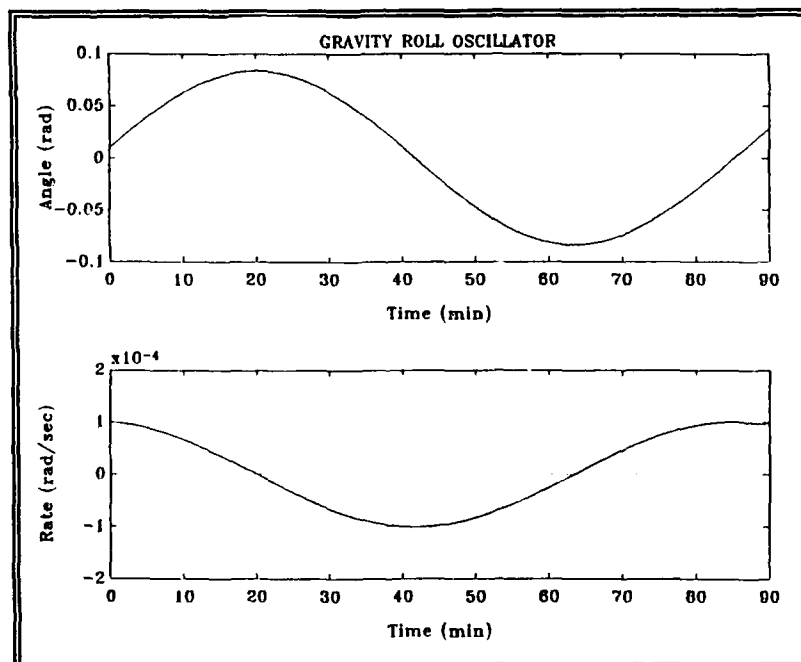


Figure 5-21b Gravitational Roll Effects Time Response

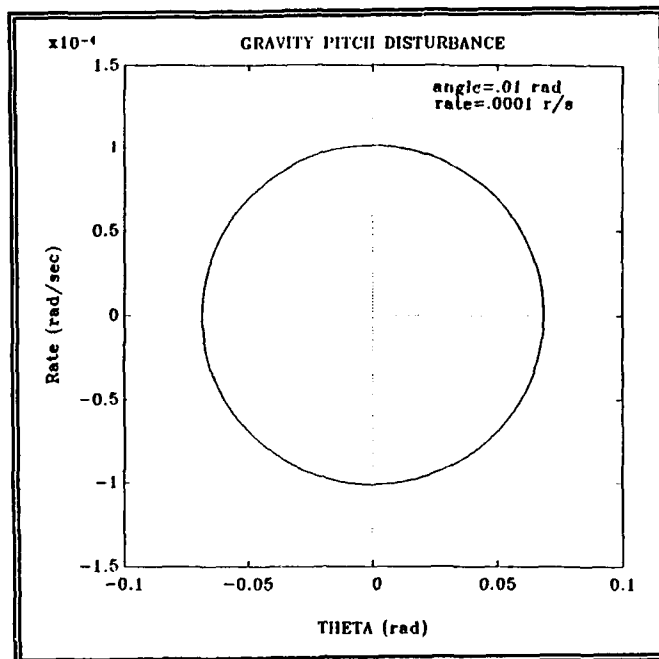


Figure 5-22a Gravitational Pitch Effects Phase Plane

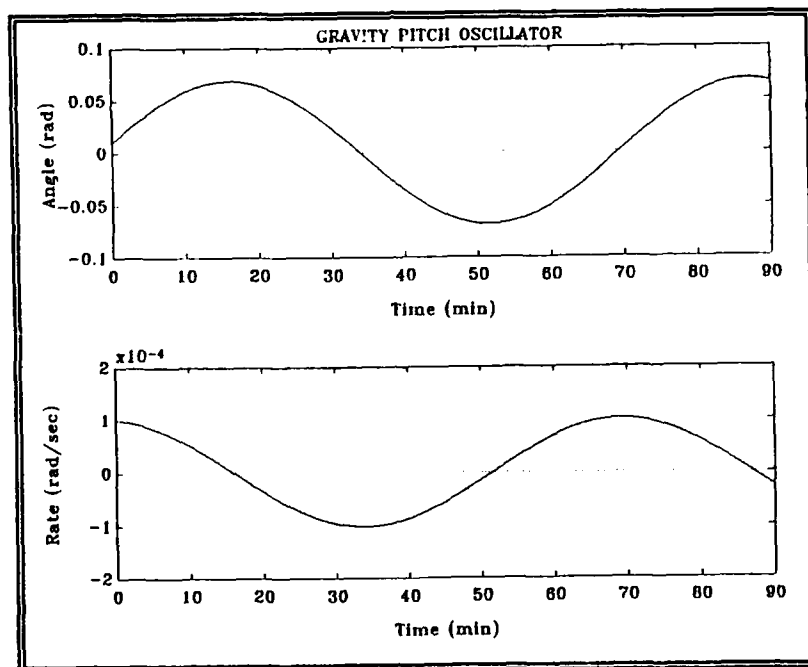


Figure 5-22b Gravitational Pitch Effects Time Response

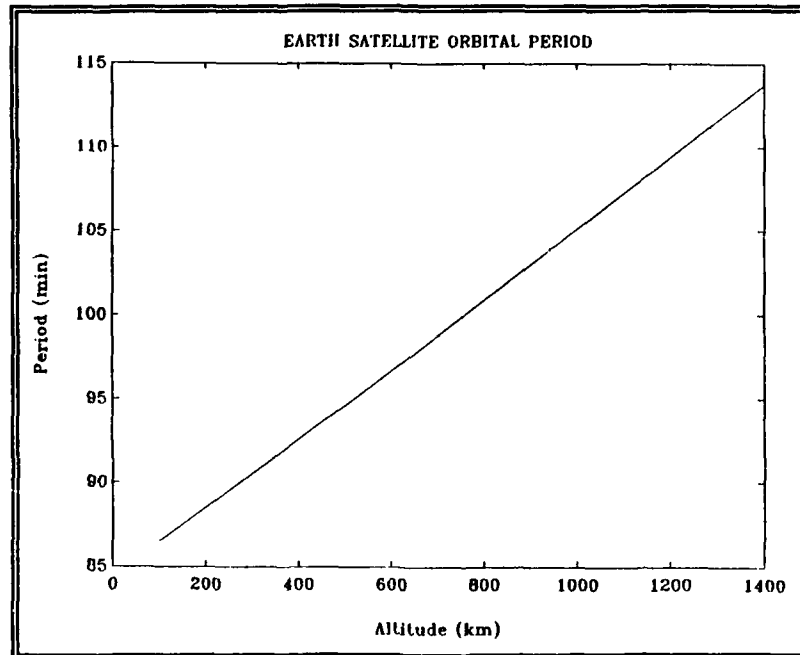


Figure 5-23 Orbital Period versus Altitude

attitude control system is on the order of 100 seconds. If the control system is operating continuously to maintain the desired pointing accuracy, then the effects of gravity are insignificant compared to the normal cycling that occurs in the limit region. If there is zero rate error and the angle error is in the limit region, the gravity gradient torque will aid in maintaining the attitude in the limit region.

The disturbance torques contributed by aerodynamic drag are

$$T_{\text{Drag}} = \begin{Bmatrix} -F_D L \sin\theta \cos\psi \\ 0 \\ F_D L \cos\theta \cos\psi \end{Bmatrix} \quad (5.37)$$

where F_D is the drag force as a function of atmospheric density. Table 5-2 lists atmospheric densities at some altitudes. [8]

Table 5-2 ATMOSPHERIC DENSITIES

Altitude(km)	Density(kg/m ³)
100	6×10^{-7}
200	7×10^{-7}
400	1×10^{-11}
1000	1×10^{-15}

At $h=400$ km the drag force is 2.52×10^{-4} Newtons. For small angles (5.37) reduces to

$$T_{Dx} = -F_D L \theta \approx -1.92 \times 10^{-5} \theta \text{ N-m}$$

$$T_{Dz} = F_D L = 1.92 \times 10^{-5} \text{ N-m}$$

where $L=.076\text{m}$ is the center of pressure offset from the center of mass. The effects of aerodynamic drag alone for an orbital period are illustrated in Figures 5-24 and 5-25 about the roll and yaw axes for initial conditions of angle=.01 rad and rate=.0001 rad/sec. The pitch angle error was assumed constant at .01 rad. The satellite response to drag is unstable, yet like gravity gradient, drag causes a slow response compared to the continuously operating all-thruster control system. Drag torques that would cause the attitude of the satellite to be unstable over the course of an orbital period do not affect motion during continuous control.

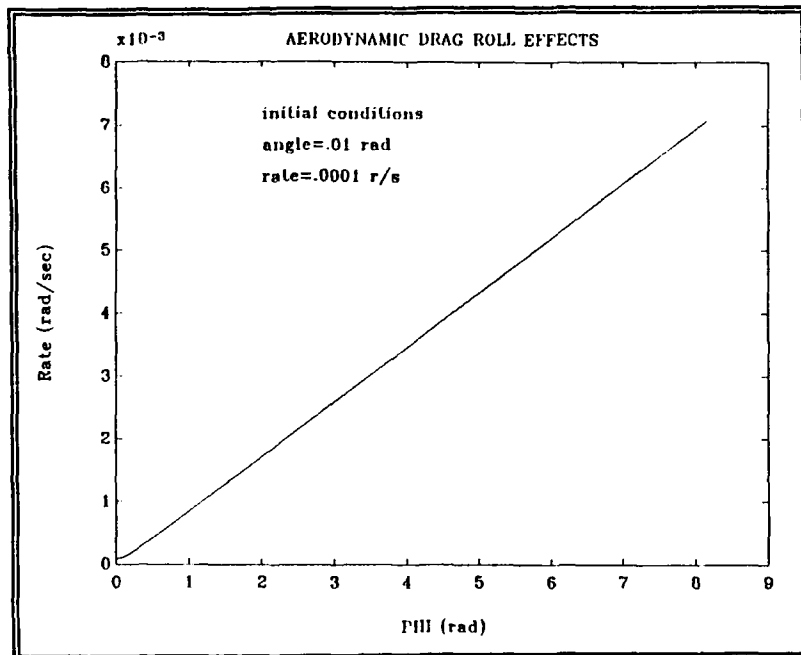


Figure 5-24a Drag Roll Effects Phase Plane

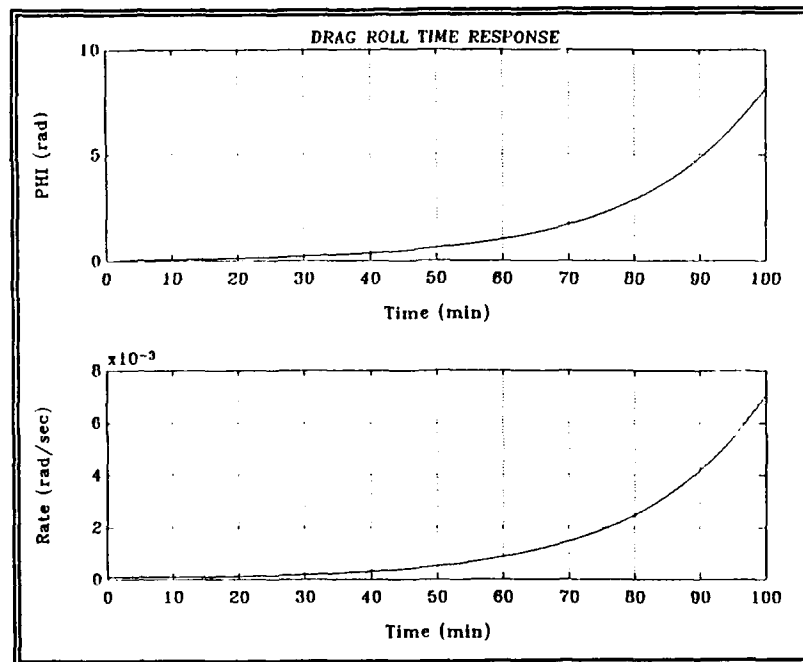


Figure 5-24b Drag Roll Effects Time Response

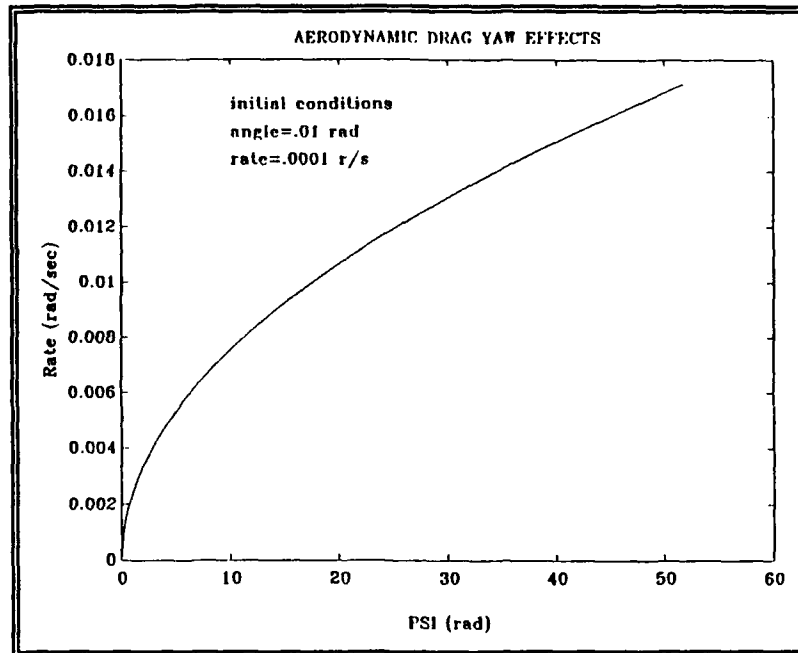


Figure 5-25a Drag Yaw Effects Phase Plane

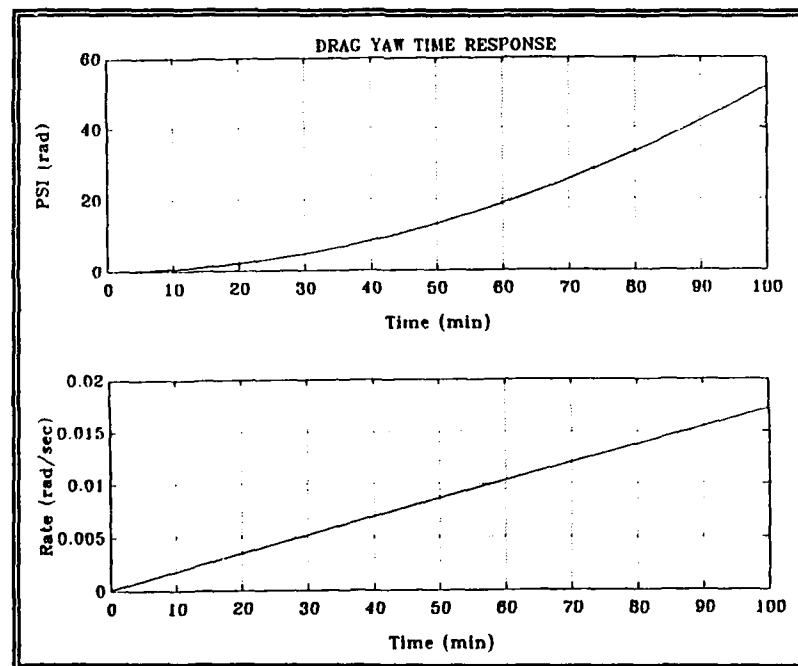


Figure 5-25b Drag Yaw Effects Time Response

Finally the effects of gravity gradient and aerodynamic drag were combined. Substituting the disturbance torques into (5.33) yields

$$\ddot{\phi} = -\alpha \omega_o^2 \phi + u_x - 2.84 \times 10^{-6} \theta \quad (5.38)$$

which is the equation of a marginally stable oscillator. The effect that gravity and drag have on roll is illustrated in Figures 5-26 and 5-27 for initial conditions of angle=.01 rad, zero rate and rate=.0001 rad/sec, respectively. The oscillation does not increase without bound and actually never repeats the same cycle. The phase plane plots have a run time of 150 minutes while the time response plots have a run time of 300 minutes. Again, the time constant of the gravity-drag torque is orders of magnitude bigger than that of the all-thruster control system. If the control system were only operated at discrete intervals during each orbit the external disturbance torques could together run the rates up to unacceptable levels.

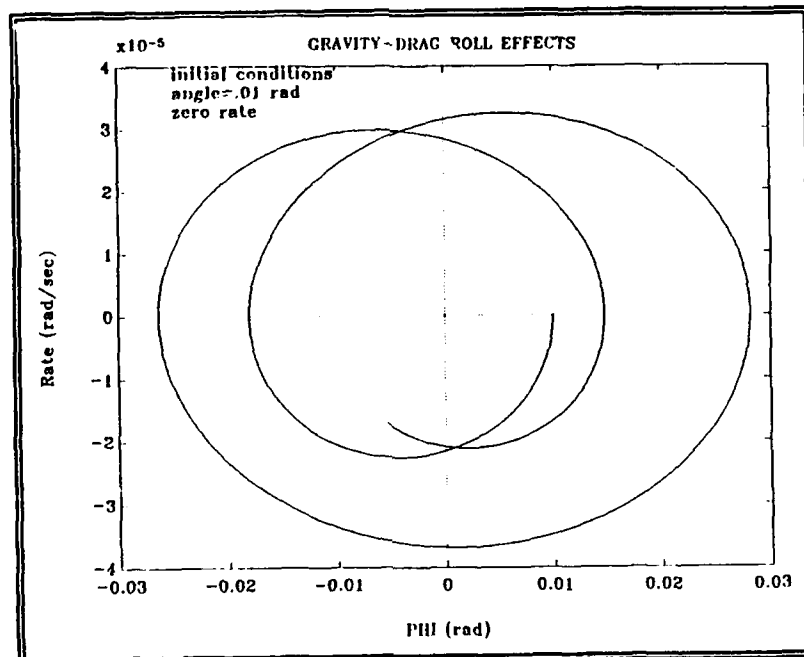


Figure 5-26a Gravity-Drag Roll Effects with Zero Rate Error Phase Plane

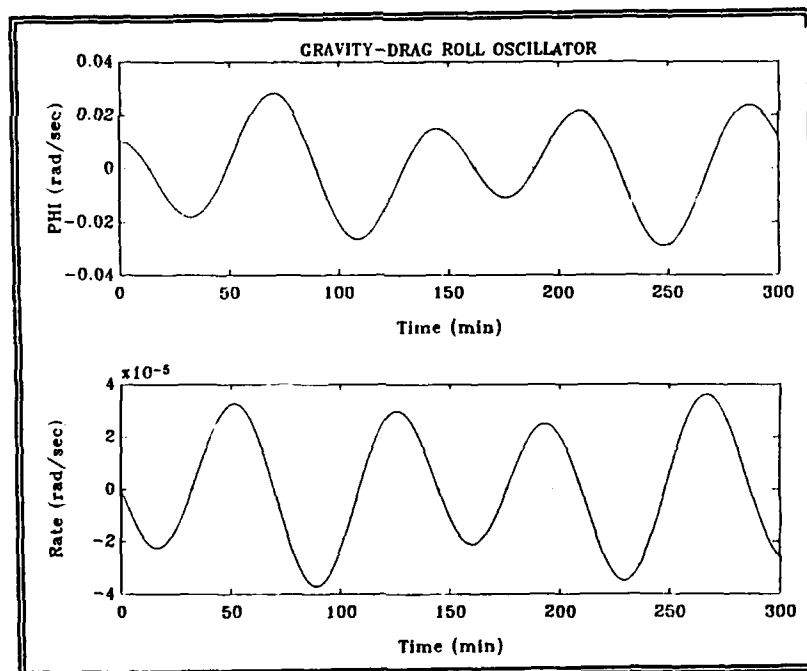


Figure 5-26b Gravity-Drag Roll Effects with Zero Rate Error Time Response

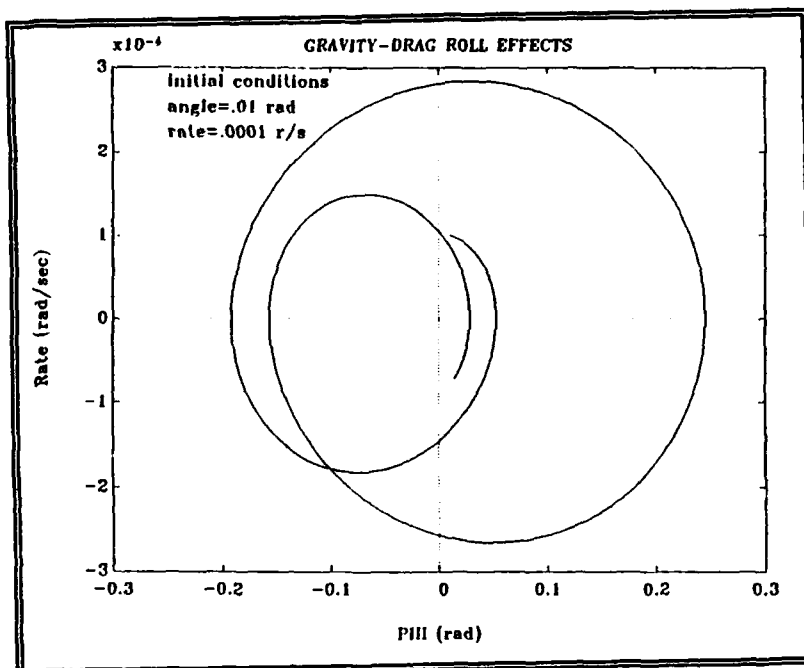


Figure 5-27a Gravity-Drag Roll Effects with Rate Error Phase Plane

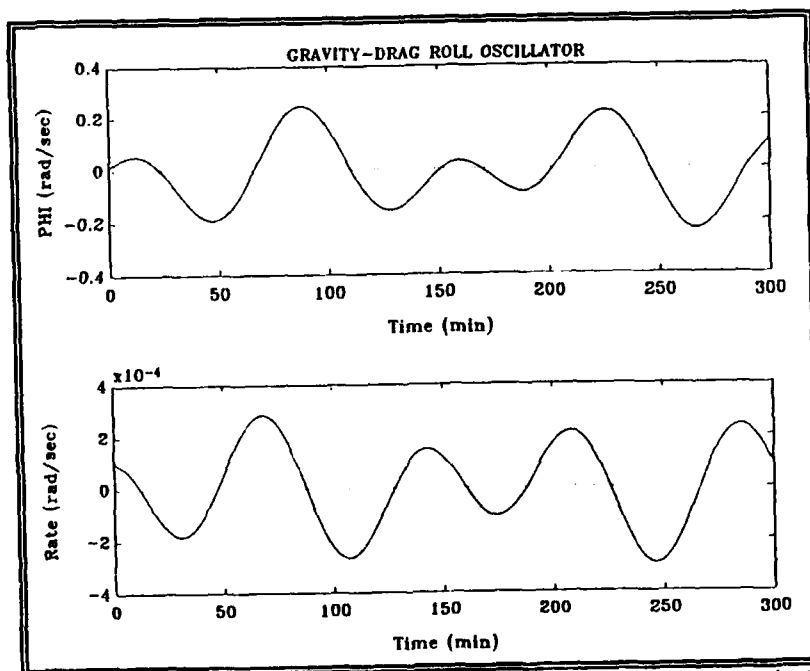


Figure 5-27b Gravity-Drag Roll Effects with Rate Error Time Response

VI. SUMMARY AND CONCLUSIONS

The purpose of this thesis was to design an all-thruster three-axis attitude control system for ORION, the Naval Postgraduate School satellite bus. Pontryagin's Minimization Principle was employed in the derivation of fuel-time minimization control laws for the acquisition and on-station phases of flight. The original design was modified slightly to accommodate a three-axis strategy.

The original design history and specifications are discussed in Chapter II. The total mass of the ORION satellite is 250 lbm including 71.5 lbm of the monopropellant hydrazine for maneuvering. The attitude control system consists primarily of one 5 lbf thruster for orbital transfer and six .1 lbf thrusters for rotational control. The original mass placement and principal moments of inertia were left unchanged for simulation purposes. The four stabilizing booms are not utilized in this analysis.

Additional concerns that affect a three-axis stabilized satellite compared to the original spin stabilized design are addressed in Chapter III. To meet power requirements, solar panels will be required vice just body-mounted solar cells. A three-axis ORION will be less fuel efficient than a spinning version. Various schemes using different combinations of

actuators are presented for future study. Alternate booster selections that could transfer ORION to higher orbits than the space shuttle and minimize the use of the 40 lbf thruster are suggested.

The theory behind satellite motion, attitude determination and control hardware for a three-axis stabilized spacecraft, is developed in Chapter IV. Rigid-body spacecraft dynamics and the effects of the environmental disturbances of gravity gradient and aerodynamic drag are covered. Attitude control sensors and actuators are described with an emphasis on the higher degree of complexity required of these instruments vice those used on a spinning satellite. Sensors include horizon sensors, sun sensors, magnetometers, and rate gyros while the actuators are strictly thrusters.

The derivation and simulation of the control laws that describe the acquisition and on-station phases of flight is found in Chapter V. It was determined that a dual-axis minimum time control law was optimal for reducing the rates as quickly as possible in the acquisition phase. Once the rates are reduced to acceptable levels, a fuel-time control law is implemented that utilizes a weighting factor to minimize fuel usage.

Two regions of interest developed during the analysis of the fuel-time control law. The boundary region is a rectangular area centered about the desired position. The

deadzone is determined by the nominal pointing accuracy ($\pm 1^\circ$ ORION design goal) in angle and the minimum thruster impulse bit for rate. The boundary region is distinguished by a four pulse limit cycle that repeats itself every 50-200 seconds for ORION. Assuming that $2/3$ of the total hydrazine budget is available for limit cycle maintenance, lifetimes of 4-28 months were obtained with all thrusters operating. The limiting factor for the selected thrusters was the number of pulses available before the Shell 405 catalyst lost effectiveness. The limit cycle lifetime decreased to 30-90 days. The second region of interest was outside the boundary region, but close enough for the satellite to still experience independent or uncoupled motion about one or more axes. A double switching curve control law distinguished by "bang-off-bang" control was realized successfully.

The environmental disturbances of gravity gradient and aerodynamic drag were also simulated in Chapter V. The gravity gradient disturbance imitates a simple harmonic oscillator with a period corresponding to an orbital period. A typical orbital period for a low earth orbit is on the order of 90 minutes. Aerodynamic drag applies an unstable torque, but when coupled with gravity causes a random but marginally stable type of oscillation. Both disturbance torques are so small over the course of a limit control cycle, that the effects are negligible.

The three-axis stabilized design simulated in this thesis could be a viable attitude control option for the general purpose ORION bus. Upgraded thrusters must be selected that have smaller minimum impulse bit on-times and thrust values in addition to an increased catalyst lifetime if ORION is to operate in the constant update control mode for a feasible duration. Another possibility that is only mentioned in this work, concerns intermittent operation. ORION could function for specified periods every orbit when the desired target is in the field of view. This method would insure an extended lifetime, but the influence of external torques could be a limiting factor.

APPENDIX

ATTITUDE CONTROL AND EXTERNAL DISTURBANCE PROGRAMS

The following programs simulate a three-axis stabilized satellite in the acquisition and on-station phases. The effects of gravity gradient and aerodynamic drag are modeled in separate routines.

The software package TUTSIM™ was used to execute the control laws derived in Chapter V [11]. TUTSIM™ models continuous time control systems in a signal flow format. The following commands are defined for the potential user:

- INT - integrator block
- CON - constant block
- GAI - gain block
- MUL - multiplier block
- DIV - divide block
- ABS - absolute value block
- AND - logical and block
- OR - logical or block
- IFE - If-then statement
- REL - relay block

The numbers preceding commands are simply block identifiers. The numbers following commands are block inputs. The constant block does not have an input. The integrator and gain blocks require at least one input. The multiply, divide and logical operator blocks need at least two inputs. The if-then statement has three inputs. The first input is the argument. The second and third inputs are the commands that support true

or false arguments, respectively. The relay block has four inputs. The last input is the argument. The first three inputs are commands that support greater than, equal to or less than results, respectively. Further information on the capabilities of TUTSIMTM can be found in the operator manual.

The first program simulates on-station control about one axis. Input parameters include initial conditions, principal moments of inertia, control torques, limit region boundary values and weighting factors for two switching curves. The command logic applies control according to the satellite attitude in the phase plane in relation to the switching curves and boundary limits. The control law for this program is derived in the first section of Chapter V.

The next three programs simulate the acquisition phase for single and double axis control. Input parameters include initial conditions for rate errors, principal moments of inertia and torque values. These programs apply control as a function of the rates for coupled equations of motion. Switching occurs about the ordinate and abscissa in a defined outer region. Switching occurs on minimum time curves in the inner region. The control law for the acquisition routines can be found in the second section of Chapter V.

The last two programs simulate the effects of gravity gradient and aerodynamic drag disturbances, respectively. Inputs parameters are provided for initial conditions,

principal moments of inertia and orbital altitude. The last section of Chapter V illustrates the effects of external disturbances.

1 INT	2			;X1,ANGLE
2 INT	39			;X2,ANGLE RATE
3 CON				;Ix,Iy,or Iz
4 CON				;Tx,Ty,or Tz
5 DIV	4	3		;Ux,Uy,or Uz
6 CON				;.5
7 CON				;1
8 CON				;4
9 ABS	1			;ABSOLUTE ANGLE
10 ABS	2			;ABSOLUTE RATE
11 CON				;ANGLE LIMIT
12 CON				;RATE LIMIT
13 CON				;LAMDA1
14 CON				;LAMDA2
15 MUL	8	13		;4*LAMDA1
16 MUL	8	14		;4*LAMDA2
17 SUM	7	15		;1+4*LAMDA1
18 SUM	7	16		;1+4*LAMDA2
19 DIV	6	5		;.5/U
20 MUL	19	17		;.5(1+4*LAMDA1)/U
21 MUL	19	18		;.5(1+4*LAMDA2)/U
22 MUL	6	10	2	;.5X2[X2]
23 MUL	20	10	2	;A1*X2[X2]
24 MUL	21	10	2	;A2*X2[X2]
25 SUM	1	22		;X1+.5X2[X2]
26 SUM	1	23		;X1+A1*X2[X2]
27 SUM	1	24		;X1+A2*X2[X2]
28 MUL	1	2		;X1*X2
29 SUM	11	-9		;X1<ANGLE LIMIT
30 SUM	12	-10		;X2<RATE LIMIT
31 GAI	5			; -Ux, -Uy or -Uz
32 REL	5	31	31	;U*SIGN(X1)
	1			
33 REL	5	31	31	;U*SIGN(X2)
	2			
34 AND	29	30		;X1<ANG LIM AND X2<RATE LIM
35 MUL	25	32		;ABOVE OR BELOW MIN TIME CURVE
36 MUL	26	32		;ABOVE OR BELOW 2nd CURVE
37 MUL	27	32		;ABOVE OR BELOW 3rd CURVE
38 CON				;U=0
39 IFE	34	38	40	;ATTITUDE IN LIMIT REGION?
40 IFE	28	-32	41	;ATTITUDE IN 1st/3rd QUADRANT?
41 IFE	29	42	43	;X1<ANGLE LIMIT?
42 IFE	37	33	44	;RELATION TO 3rd CURVE?
43 IFE	36	33	44	;RELATION TO 2nd CURVE?
44 IFE	35	38	-33	;RELATION TO MIN TIME CURVE?

1 On-Station Control

1	INT	3				;Wx
2	INT	4	27			;Wz
3	MUL	1	2	8		;(Iy-Iz)/Ix*Wy*Wz
4	MUL	18	1	8		;(Ix-Iy)/Iz*Wy*Wx
5	ABS	1				;ABSOLUTE ROLL RATE
6	ABS	2				;ABSOLUTE YAW RATE
7	CON					;.5
8	CON					;Wy=.01
9	CON					;Ix
10	CON					;Iy
11	CON					;Iz
12	CON					;Tz
13	DIV	12	11			;Uz
14	GAI	13				;-Uz
15	SUM	10	-11			;Iy-Iz
16	SUM	9	-10			;Ix-Iy
17	DIV	15	9			;(Iy-Iz)/Ix
18	DIV	16	11			;(Ix-Iy)/Iz
19	MUL	7	2	6		;.5Wz[Wz]
20	MUL	-7	1	5		;- .5Wx[Wx]
21	SUM	1	20	19		;Wx-.5Wx[Wx]+.5Wz[Wz]
22	MUL	1	1			;Wx^2
23	MUL	2	2			;Wz^2
24	MUL	29	13	13		;4*Uz^2
25	SUM	22	23	-24		;Wx^2+Wz^2>4*Uz^2
26	REL	14	13	13		;U=-U*SIGN(Wx-.5Wx[Wx]+.5Wz[Wz])
		21				
27	IFE	25	28	26		;INNER CONTROL
28	IFE	2	14	13		;OUTER CONTROL
29	CON					;4

2 Acquisition Control for a Single Actuator Set, Uz

1	INT	3	27		;Wx
2	INT	4			;Wz
3	MUL	17	2	8	;(Iy-Iz)/Ix*Wy*Wz
4	MUL	18	1	8	;(Ix-Iy)/Iz*Wy*Wx
5	ABS	1			;ABSOLUTE ROLL RATE
6	ABS	2			;ABSOLUTE YAW RATE
7	CON				;.5
8	CON				;Wy-.01
9	CON				;Ix
10	CON				;Iy
11	CON				;Iz
12	CON				;Tx
13	DIV	12	9		;Ux
14	GAI	13			;-Ux
15	SUM	10	-11		;Iy-Iz
16	SUM	9	-10		;Ix-Iy
17	DIV	15	9		;(Iy-Iz)/Ix
18	DIV	16	11		;(Ix-Iy)/Iz
19	MUL	7	2	6	;.5Wz{Wz}
20	MUL	7	1	5	;.5Wx{Wx}
21	SUM	-2	19	20	;-Wz+.5Wx{Wx}+.5Wz{Wz}
22	MUL	1	1		;Wx^2
23	MUL	2	2		;Wz^2
24	MUL	29	13	13	;4*Ux^2
25	SUM	22	23	-24	;Wx^2+Wz^2>4*Ux^2
26	REL	14	13	13	;U=-U*SIGN(-Wz+.5Wx{Wx}+.5Wz{Wz
		21			
27	IFE	25	28	26	;INNER CONTROL
28	IFE	1	14	13	;OUTER CONTROL
29	CON				;4

3 Acquisition Control for a Single Actuator Set, Ux

1	INT	3	35		;Wx
2	INT	4	36		;Wz
3	MUL	20	2	8	;(Iy-Iz)/Ix*Wy*Wz
4	MUL	21	1	8	;(Ix-Iy)/Iz*Wy*Wx
5	ABS	1			;ABSOLUTE ROLL RATE
6	ABS	2			;ABSOLUTE YAW RATE
7	CON				;.5
8	CON				;Wy=.01
9	CON				;Ix
10	CON				;Iy
11	CON				;Iz
12	CON				;Tx
13	CON				;Tz
14	DIV	12	9		;Ux
15	GAI	14			;-Ux
16	DIV	13	11		;Uz
17	GAI	16			;-Uz
18	SUM	10	-11		;Iy-Iz
19	SUM	9	-10		;Ix-Iy
20	DIV	18	9		;(Iy-Iz)/Ix
21	DIV	19	11		;(Ix-Iy)/Iz
22	MUL	7	1	5	;.5Wx[Wx]
23	MUL	7	2	6	;.5Wz[Wz]
24	SUM	1	2	-22	;Wx+Wz-.5Wx[Wx]+.5Wz[Wz]
		23			
25	SUM	1	-2	22	;Wx-Wz+.5Wx[Wx]+.5Wz[Wz]
		23			
26	REL	17	16	16	;-Uz*SIGN(25)
		25			
27	REL	15	14	14	;-Ux*SIGN(24)
		24			
28	MUL	1	1		;Wx^2
29	MUL	2	2		;Wz^2
30	CON				;-4
31	MUL	14	14	30	;-4*U^2
32	SUM	28	29	31	;Wx^2+Wz^2>4*U^2
33	REL	17	16	16	;Uz--Uz*SIGN(Wx)
		1			
34	REL	15	14	14	;Ux--Ux*SIGN(Wz)
		2			
35	IFE	32	33	26	;Uz
36	IFE	32	34	27	;Ux

4 Acquisition Control for a Double Actuator

1	INT	2			; PHI
2	INT	20			; D(PHI)/DT
3	INT	4			; THETA
4	INT	21			; D(THETA)/DT
5	CON				; Ix
6	CON				; Iy
7	CON				; Iz
8	CON				; GRAVITATIONAL PARAMETER=3.986e5
9	CON				; HEIGHT
10	CON				; EARTH RADIUS=6378 KM
11	SUM	9	10		; R=Re+H
12	CON				; -2
13	CON				; 3
14	SUM	6	-7		; Iy-Iz
15	SUM	7	-5		; Iz-Ix
16	DIV	14	5		; (Iy-Iz)/Ix
17	DIV	15	6		; (Iz-Ix)/Iy
18	MUL	11	11	11	; R^3
19	DIV	8	18		; ORBITAL RATE, Wo^2=MU/R^3
20	MUL	12	19	16	; -2 Wo^2 (Iy-Iz)/Ix*PHI
		1			
21	MUL	13	19	17	; 3 Wo^2 (Iz-Ix)/Iy*THETA
		3			

5 Gravity Gradient Disturbance Effects

1 INT	2			; PHI
2 INT	26	28		; D(PHI)/DT
3 INT	4			; PSI
4 INT	27			; D(PSI)/DT
5 CON				; Ix
6 CON				; Iy
7 CON				; Iz
8 CON				; GRAVITATIONAL PARAMETER=3.986e5
9 CON				; EARTH RADIUS=6378 KM
10 CON				; HEIGHT
11 SUM	9	10		; R=Re+H
12 SUM	6	-7		; Iy-Iz
13 DIV	12	5		; (Iy-Iz)/Ix
14 CON				; DENSITY,RHO
15 CON				; ORION CROSS-SECTION,A=.429m^2
16 CON				; .5
17 CON				; DRAG COEFFICIENT=2
18 DIV	8	11		; ORBITAL VELOCITY,V^2
19 MUL	16	14	30	; DRAG FORCE
	17	15		
20 CON				; L=.076 m
21 MUL	11	11	11	; R^3
22 DIV	8	21		; ORBITAL RATE,Wo^2
23 MUL	19	20		; DRAG YAW TORQUE
24 CON				; THETA
25 MUL	-23	24		; DRAG ROLL TORQUE
26 MUL	13	22	1	; Wo^2 (Iy-Iz)/Ix*PHI
27 DIV	23	7		; FD*L/Iz
28 DIV	25	5		; FD*L*THETA/Ix
29 CON				; 1e6
30 MUL	18	29		; V^2 IN M^2/S^2

6 Aerodynamic Drag Disturbance Effects

LIST OF REFERENCES

1. Boyd, Austin W., *Design Considerations for the ORION Satellite: Structure, Propulsion and Attitude Control Subsystems for a Small, General Purpose Spacecraft*, M.S.E.E. Thesis, Naval Postgraduate School, Monterey, California, March 1988
2. Agrawal, Brij N., *Design of Geosynchronous Spacecraft*, pp.105-178, Prentice-Hall Inc., 1986
3. Cippolone, Lawrence V., Lyon, David C., *Launch Alternatives for Small Satellites and the Current Commercial, Political and Physical Environments*, pp.104-390, M.S.S.T. Thesis, Naval Postgraduate School, Monterey, California, September 1988
4. Bate, Roger R., Mueller, Donald D., White, Jerry E., *Fundamentals of Astrodynamics*, pp.1-177, Dover Publications Inc., 1971
5. Ha, Tri T., *Digital Satellite Communications*, pp.31-69, Macmillan Publishing Company, 1986

6. Falb, Peter L., Athanassiades, Michael, *Time Optimal Velocity Control of a Spinning Space Body*, Massachusetts Institute of Technology, Lincoln Laboratory Report 22G-8, September 1962
7. Wertz, James R., *Spacecraft Attitude Determination and Control*, pp.13-216, D. Reidel Publishing Company, 1986
8. Chappel, David C., *Preliminary Design of the ORION Attitude Control System*, M.S.E.E. Thesis, Naval Postgraduate School, Monterey, California, December 1987
9. Kirk, Donald E., *Optimal Control Theory*, pp.184-325, Prentice-Hall Inc., 1970
10. Kaplan, Marshall H., *Modern Spacecraft Dynamics and Control*, pp.152-211, John Wiley & Sons, 1976
11. Reynolds, Walter E., Wolf, Jinner, *TUTSIMTM Users Manual IBM* MS-DOS Version*, TUTSIMTM Products, Palo Alto, California, 1988
12. Schroeder, Douglas S., *Applications of ORION to Navy UHF Satellite Communications*, M.S.E.E. Thesis, Naval Postgraduate School, Monterey, California, December 1987

INITIAL DISTRIBUTION LIST

	No. of Copies
1. Defense Technical Information Center Cameron Station Alexandria, VA 22304-6145	2
2. Library, Code 0142 Naval Postgraduate School Monterey, CA 93943-5002	2
3. Dr. Hal A. Titus Code 62TI Monterey, CA 93943-5000	4
4. Professor Jeffrey Burl Code 62BI Monterey, CA 93943-5000	1
5. Space Systems Academic Group Attn: Dr. Rudolph Panholzer Code 72 Monterey, CA 93943-5000	1
6. Distinguished Professor Allen E. Fuhs P.O. Box 3258 Monterey, CA 93942	1
7. Chairman, Dept. of Electrical & Computer Engineering Code 62 Monterey, CA 93943-5000	1
8. Director of Research Administration Code 012 Monterey, CA 93943-5000	1
9. United States Space Command Attn: Technical Library Peterson AFB, CO 80914	1
10. Naval Space Command Code N3 Dahlgren, VA 22448	2

- | | |
|---|---|
| 11. Commander
Naval Space Surveillance Activity
Dahlgren, VA 22448 | 1 |
| 12. Director, Navy Space Systems Division
Chief of Naval Operations
(OP-943)
Washington, DC 20305-2006 | 1 |
| 13. Commander
Space and Naval Warfare Systems Command
(PD-80)
Washington, DC 20361-5100 | 1 |
| 14. LT Suzanne Dee
Naval Space Surveillance Activity
Dahlgren, VA 22448 | 2 |
| 15. Marv Levenson
Naval Research Labrotory
Code 8231
4555 Overlook Ave. S.W.
Washington, D.C. 20375 | 1 |
| 16. Marty Mosier
Orbital Sciences Corporation
12500 Fair Lakes Circle, Suite 350
Fairfax, VA 22033 | 1 |
| 17. LCDR Austin Boyd
NMPC, Sea Duty Component
P.O. Box 16134
Arlington, VA 22215-1134 | 1 |